The Astrophysical Journal Letters, 896:L44 (20pp), 2020 June 20 https://doi.org/10.3847/2041-8213/ab960f

GW190814: Gravitational Waves from the Coalescence of a 23 Solar Mass Black Hole with a 2.6 Solar Mass Compact Object

R. Abbott[1], T. D. Abbott[2], S. Abraham[3], F. Acernese[4,5], K. Ackley[6], C. Adams[7], R. X. Adhikari[1], V. B. Adya[8], C. Affeldt[9,10], M. Agathos[11,12], K. Agatsuma[13], N. Aggarwal[14], O. D. Aguiar[15], A. Aich[16], L. Aiello[17,18], A. Ain[3], P. Ajith[19], S. Akcay[11,20], G. Allen[21], A. Allocca[22], P. A. Altin[8], A. Amato[23], S. Anand[1], A. Ananyeva[1], S. B. Anderson[1], W. G. Anderson[24], S. V. Angelova[25], S. Ansoldi[26,27], S. Antier[28], S. Appert[1], K. Arai[1], M. C. Araya[1], J. S. Areeda[29], M. Arène[28], N. Arnaud[30,31], S. M. Aronson[32], K. G. Arun[33], Y. Asali[34], S. Ascenzi[17,35], G. Ashton[6], S. M. Aston[7], P. Astone[36], F. Aubin[37], P. Aufmuth[10], K. AultONeal[38], C. Austin[2], V. Avendano[39], S. Babak[28], P. Bacon[28], F. Badaracco[17,18], M. K. M. Bader[40], S. Bae[41], A. M. Baer[42], J. Baird[28], F. Baldaccini[43,44], G. Ballardin[31], S. W. Ballmer[45], A. Bals[38], A. Balsamo[42], G. Baltus[46], S. Banagiri[47], D. Bankar[3], R. S. Bankar[3], J. C. Barayoga[1], C. Barbieri[48,49], B. C. Barish[1], D. Barker[50], K. Barkett[51], P. Barneo[52], F. Barone[5,53], B. Barr[54], L. Barsotti[55], M. Barsuglia[28], D. Barta[56], J. Bartlett[50], I. Bartos[32], R. Bassiri[57], A. Basti[22,58], M. Bawaj[44,59], J. C. Bayley[54], M. Bazzan[60,61], B. Bécsy[62], M. Bejger[63], I. Belahcene[30], A. S. Bell[54], D. Beniwal[64], M. G. Benjamin[38], R. Benkel[65], J. D. Bentley[13], F. Bergamin[9], B. K. Berger[57], G. Bergmann[9,10], S. Bernuzzi[11], C. P. L. Berry[14], D. Bersanetti[66], A. Bertolini[40], J. Betzwieser[7], R. Bhandare[67], A. V. Bhandari[3], J. Bidler[29], E. Biggs[24], I. A. Bilenko[68], G. Billingsley[1], R. Birney[69], O. Birnholtz[70,71], S. Biscans[1,55], M. Bischi[72,73], S. Biscoveanu[55], A. Bisht[10], G. Bissenbayeva[16], M. Bitossi[22,31], M. A. Bizouard[74], J. K. Blackburn[1], J. Blackman[51], C. D. Blair[7], D. G. Blair[75], R. M. Blair[50], F. Bobba[76,77], N. Bode[9,10], M. Boer[74], Y. Boetzel[78], G. Bogaert[74], F. Bondu[79], E. Bonilla[57], R. Bonnand[37], P. Booker[9,10], B. A. Boom[40], R. Bork[1], V. Boschi[22], S. Bose[3], V. Bossilkov[75], J. Bosveld[75], Y. Bouffanais[60,61], A. Bozzi[31], C. Bradaschia[22], P. R. Brady[24], A. Bramley[7], M. Branchesi[17,18], J. E. Brau[80], M. Breschi[11], T. Briant[81], J. H. Briggs[54], F. Brighenti[72,73], A. Brillet[74], M. Brinkmann[9,10], R. Brito[36,65,82], P. Brockill[24], A. F. Brooks[1], J. Brooks[31], D. D. Brown[64], S. Brunett[1], G. Bruno[83], R. Bruntz[42], A. Buikema[55], T. Bulik[84], H. J. Bulten[40,85], A. Buonanno[65,86], D. Buskulic[37], R. L. Byer[57], M. Cabero[9,10], L. Cadonati[87], G. Cagnoli[88], C. Cahillane[1], J. Calderón Bustillo[6], J. D. Callaghan[54], T. A. Callister[1], E. Calloni[5,89], J. B. Camp[90], M. Canepa[66,91], K. C. Cannon[92], H. Cao[64], J. Cao[93], G. Carapella[76,77], F. Carbognani[31], S. Caride[94], M. F. Carney[14], G. Carullo[22,58], J. Casanueva Diaz[22], C. Casentini[35,95], J. Castañeda[52], S. Caudill[40], M. Cavaglià[96], F. Cavalier[30], R. Cavalieri[31], G. Cella[22], P. Cerdá-Durán[97], E. Cesarini[35,98], O. Chaibi[74], K. Chakravarti[3], C. Chan[92], M. Chan[54], S. Chao[99], P. Charlton[100], E. A. Chase[14], E. Chassande-Mottin[28], D. Chatterjee[24], M. Chaturvedi[67], K. Chatziioannou[101,102], H. Y. Chen[103], X. Chen[75], Y. Chen[51], H.-P. Cheng[32], C. K. Cheong[104], H. Y. Chia[32], F. Chiadini[77,105], R. Chierici[106], A. Chincarini[66], A. Chiummo[31], G. Cho[107], H. S. Cho[108], M. Cho[86], N. Christensen[74], Q. Chu[75], S. Chua[81], K. W. Chung[104], S. Chung[75], G. Ciani[60,61], P. Ciecielag[63], M. Cieślar[63], A. A. Ciobanu[64], R. Ciolfi[61,109], F. Cipriano[74], A. Cirone[66,91], F. Clara[50], J. A. Clark[87], P. Clearwater[110], S. Clesse[83], F. Cleva[74], E. Coccia[17,18], P.-F. Cohadon[81], D. Cohen[30], M. Colleoni[111], C. G. Collette[112], C. Collins[13], M. Colpi[48,49], M. Constancio, Jr.[15], L. Conti[61], S. J. Cooper[13], P. Corban[7], T. R. Corbitt[2], I. Cordero-Carrión[113], S. Corezzi[43,44], K. R. Corley[34], N. Cornish[62], D. Corre[30], A. Corsi[94], S. Cortese[31], C. A. Costa[15], R. Cotesta[65], M. W. Coughlin[1], S. B. Coughlin[14,114], J.-P. Coulon[74], S. T. Countryman[34], P. Couvares[1], P. B. Covas[111], D. M. Coward[75], M. J. Cowart[7], D. C. Coyne[1], R. Coyne[115], J. D. E. Creighton[24], T. D. Creighton[16], J. Cripe[2], M. Croquette[81], S. G. Crowder[116], J.-R. Cudell[46], T. J. Cullen[2], A. Cumming[54], R. Cummings[54], L. Cunningham[54], E. Cuoco[31], M. Curylo[84], T. Dal Canton[65], G. Dálya[117], A. Dana[57], L. M. Daneshgaran-Bajastani[118], B. D'Angelo[66,91], S. L. Danilishin[9,10], S. D'Antonio[35], K. Danzmann[9,10], C. Darsow-Fromm[119], A. Dasgupta[120], L. E. H. Datrier[54], V. Dattilo[31], I. Dave[67], M. Davier[30], G. S. Davies[121], D. Davis[45], E. J. Daw[122], D. DeBra[57], M. Deenadayalan[3], J. Degallaix[23], M. De Laurentis[5,89], S. Deléglise[81], M. Delfavero[70], N. De Lillo[54], W. Del Pozzo[22,58], L. M. DeMarchi[14], V. D'Emilio[114], N. Demos[55], T. Dent[121], R. De Pietri[123,124], R. De Rosa[5,89], C. De Rossi[31], R. DeSalvo[125], O. de Varona[9,10], S. Dhurandhar[3], M. C. Díaz[16], M. Diaz-Ortiz, Jr.[32], T. Dietrich[40], L. Di Fiore[5], C. Di Fronzo[13], C. Di Giorgio[76,77], F. Di Giovanni[97], M. Di Giovanni[126,127], T. Di Girolamo[5,89], A. Di Lieto[22,58], B. Ding[112], S. Di Pace[36,82], I. Di Palma[36,82], F. Di Renzo[22,58], A. K. Divakarla[32], A. Dmitriev[13], Z. Doctor[103], F. Donovan[55], K. L. Dooley[114], S. Doravari[3], I. Dorrington[114], T. P. Downes[24], M. Drago[17,18], J. C. Driggers[50], Z. Du[93], J.-G. Ducoin[30], P. Dupej[54], O. Durante[76,77], D. D'Urso[128,129], S. E. Dwyer[50], P. J. Easter[6], G. Eddolls[54], B. Edelman[80], T. B. Edo[122], O. Edy[130], A. Effler[7], P. Ehrens[1], J. Eichholz[8], S. S. Eikenberry[32], M. Eisenmann[37], R. A. Eisenstein[55], A. Ejlli[114], L. Errico[5,89], R. C. Essick[103], H. Estelles[111], D. Estevez[37], Z. B. Etienne[131], T. Etzel[1], M. Evans[55], T. M. Evans[7], B. E. Ewing[132], V. Fafone[17,35,95], S. Fairhurst[114], X. Fan[93], S. Farinon[66], B. Farr[80], W. M. Farr[101,102], E. J. Fauchon-Jones[114], M. Favata[39], M. Fays[122], M. Fazio[133], J. Feicht[1], M. M. Fejer[57], F. Feng[28], E. Fenyvesi[56,134], D. L. Ferguson[87], A. Fernandez-Galiana[55], I. Ferrante[22,58], E. C. Ferreira[15], T. A. Ferreira[15], F. Fidecaro[22,58], I. Fiori[31], D. Fiorucci[17,18], M. Fishbach[103], R. P. Fisher[42], R. Fittipaldi[77,135], M. Fitz-Axen[47], V. Fiumara[77,136], R. Flaminio[37,137], E. Floden[47], E. Flynn[29], H. Fong[92], J. A. Font[97,138], P. W. F. Forsyth[8], J.-D. Fournier[74], S. Frasca[36,82], F. Frasconi[22], Z. Frei[117], A. Freise[13], R. Frey[80], V. Frey[30], P. Fritschel[55], V. V. Frolov[7], G. Fronzè[139], P. Fulda[32], M. Fyffe[7], H. A. Gabbard[54], B. U. Gadre[65], S. M. Gaebel[13], J. R. Gair[65], S. Galaudage[6], D. Ganapathy[55], A. Ganguly[19], S. G. Gaonkar[3], C. García-Quirós[111], F. Garufi[5,89], B. Gateley[50], S. Gaudio[38], V. Gayathri[140], G. Gemme[66], E. Genin[31], A. Gennai[22], D. George[21], J. George[67], L. Gergely[141], S. Ghonge[87], Abhirup Ghosh[65], Archisman Ghosh[40,142,143,144], S. Ghosh[24], B. Giacomazzo[126,127], J. A. Giaime[2,7], K. D. Giardina[7],

D. R. Gibson[69], C. Gier[25], K. Gill[34], J. Glanzer[2], J. Gniesmer[119], P. Godwin[132], E. Goetz[2,96], R. Goetz[32], N. Gohlke[9,10], B. Goncharov[6], G. González[2], A. Gopakumar[145], S. E. Gossan[1], M. Gosselin[22,31,58], R. Gouaty[37], B. Grace[8], A. Grado[5,146], M. Granata[23], A. Grant[54], S. Gras[55], P. Grassia[1], C. Gray[50], R. Gray[54], G. Greco[72,73], A. C. Green[32], R. Green[114], E. M. Gretarsson[38], H. L. Griggs[87], G. Grignani[43,44], A. Grimaldi[126,127], S. J. Grimm[17,18], H. Grote[114], S. Grunewald[65], P. Gruning[30], G. M. Guidi[72,73], A. R. Guimaraes[2], G. Guixé[52], H. K. Gulati[120], Y. Guo[40], A. Gupta[132], Anchal Gupta[1], P. Gupta[40], E. K. Gustafson[1], R. Gustafson[147], L. Haegel[111], O. Halim[17,18], E. D. Hall[55], E. Z. Hamilton[114], G. Hammond[54], M. Haney[78], M. M. Hanke[9,10], J. Hanks[50], C. Hanna[132], M. D. Hannam[114], O. A. Hannuksela[104], T. J. Hansen[38], J. Hanson[7], T. Harder[74], T. Hardwick[2], K. Haris[19], J. Harms[17,18], G. M. Harry[148], I. W. Harry[130], R. K. Hasskew[7], C.-J. Haster[55], K. Haughian[54], F. J. Hayes[54], J. Healy[70], A. Heidmann[81], M. C. Heintze[7], J. Heinze[9,10], H. Heitmann[74], F. Hellman[149], P. Hello[30], G. Hemming[31], M. Hendry[54], I. S. Heng[54], E. Hennes[40], J. Hennig[9,10], M. Heurs[9,10], S. Hild[54,150], T. Hinderer[40,142,144], S. Y. Hoback[29,148], S. Hochheim[9,10], E. Hofgard[57], D. Hofman[23], A. M. Holgado[21], N. A. Holland[8], K. Holt[7], D. E. Holz[103], P. Hopkins[114], C. Horst[24], J. Hough[54], E. J. Howell[75], C. G. Hoy[114], Y. Huang[55], M. T. Hübner[6], E. A. Huerta[21], D. Huet[30], B. Hughey[38], V. Hui[37], S. Husa[111], S. H. Huttner[54], R. Huxford[132], T. Huynh-Dinh[7], B. Idzkowski[84], A. Iess[35,95], H. Inchauspe[32], C. Ingram[64], G. Intini[36,82], J.-M. Isac[81], M. Isi[55], B. R. Iyer[19], T. Jacqmin[81], S. J. Jadhav[151], S. P. Jadhav[3], A. L. James[114], K. Jani[87], N. N. Janthalur[151], P. Jaranowski[152], D. Jariwala[32], R. Jaume[111], A. C. Jenkins[153], J. Jiang[32], G. R. Johns[42], N. K. Johnson-McDaniel[12], A. W. Jones[13], D. I. Jones[154], J. D. Jones[50], P. Jones[13], R. Jones[54], R. J. G. Jonker[40], L. Ju[75], J. Junker[9,10], C. V. Kalaghatgi[114], V. Kalogera[14], B. Kamai[1], S. Kandhasamy[3], G. Kang[41], J. B. Kanner[1], S. J. Kapadia[19], S. Karki[80], R. Kashyap[19], M. Kasprzack[1], W. Kastaun[9,10], S. Katsanevas[31], E. Katsavounidis[55], W. Katzman[7], S. Kaufer[10], K. Kawabe[50], F. Kéfélian[74], D. Keitel[130], A. Keivani[34], R. Kennedy[122], J. S. Key[155], S. Khadka[57], F. Y. Khalili[68], I. Khan[17,35], S. Khan[9,10], Z. A. Khan[93], E. A. Khazanov[156], N. Khetan[17,18], M. Khursheed[67], N. Kijbunchoo[8], Chunglee Kim[157], G. J. Kim[87], J. C. Kim[158], K. Kim[104], W. Kim[64], W. S. Kim[159], Y.-M. Kim[160], C. Kimball[14], P. J. King[50], M. Kinley-Hanlon[54], R. Kirchhoff[9,10], J. S. Kissel[50], L. Kleybolte[119], S. Klimenko[32], T. D. Knowles[131], E. Knyazev[55], P. Koch[9,10], S. M. Koehlenbeck[9,10], G. Koekoek[40,150], S. Koley[40], V. Kondrashov[1], A. Kontos[161], N. Koper[9,10], M. Korobko[119], W. Z. Korth[1], M. Kovalam[75], D. B. Kozak[1], V. Kringel[9,10], N. V. Krishnendu[33], A. Królak[162,163], N. Krupinski[24], G. Kuehn[9,10], A. Kumar[151], P. Kumar[164], Rahul Kumar[50], Rakesh Kumar[120], S. Kumar[19], L. Kuo[99], A. Kutynia[162], B. D. Lackey[65], D. Laghi[22,58], E. Lalande[165], T. L. Lam[104], A. Lamberts[74,166], M. Landry[50], P. Landry[29], B. B. Lane[55], R. N. Lang[167], J. Lange[70], B. Lantz[57], R. K. Lanza[55], I. La Rosa[37], A. Lartaux-Vollard[30], P. D. Lasky[6], M. Laxen[7], A. Lazzarini[1], C. Lazzaro[61], P. Leaci[36,82], S. Leavey[9,10], Y. K. Lecoeuche[50], C. H. Lee[108], H. M. Lee[168], H. W. Lee[158], J. Lee[107], K. Lee[57], J. Lehmann[9,10], N. Leroy[30], N. Letendre[37], Y. Levin[6], A. K. Y. Li[104], J. Li[93], K. li[104], T. G. F. Li[104], X. Li[51], F. Linde[40,169], S. D. Linker[118], J. N. Linley[54], T. B. Littenberg[170], J. Liu[9,10], X. Liu[24], M. Llorens-Monteagudo[97], R. K. L. Lo[1], A. Lockwood[171], L. T. London[55], A. Longo[172,173], M. Lorenzini[17,18], V. Loriette[174], M. Lormand[7], G. Losurdo[22], J. D. Lough[9,10], C. O. Lousto[70], G. Lovelace[29], H. Lück[9,10], D. Lumaca[35,95], A. P. Lundgren[130], Y. Ma[51], R. Macas[114], S. Macfoy[25], M. MacInnis[55], D. M. Macleod[114], I. A. O. MacMillan[148], A. Macquet[74], I. Magaña Hernandez[24], F. Magaña-Sandoval[32], R. M. Magee[132], E. Majorana[36], I. Maksimovic[174], A. Malik[67], N. Man[74], V. Mandic[47], V. Mangano[36,54,82], G. L. Mansell[50,55], M. Manske[24], M. Mantovani[31], M. Mapelli[60,61], F. Marchesoni[44,59,175], F. Marion[37], S. Márka[34], Z. Márka[34], C. Markakis[12], A. S. Markosyan[57], A. Markowitz[1], E. Maros[1], A. Marquina[113], S. Marsat[28], F. Martelli[72,73], I. W. Martin[54], R. M. Martin[39], V. Martinez[88], D. V. Martynov[13], H. Masalehdan[119], K. Mason[55], E. Massera[122], A. Masserot[37], T. J. Massinger[55], M. Masso-Reid[54], S. Mastrogiovanni[28], A. Matas[65], F. Matichard[1,55], N. Mavalvala[55], E. Maynard[2], J. J. McCann[75], R. McCarthy[50], D. E. McClelland[8], S. McCormick[7], L. McCuller[55], S. C. McGuire[176], C. McIsaac[130], J. McIver[1], D. J. McManus[8], T. McRae[8], S. T. McWilliams[131], D. Meacher[24], G. D. Meadors[6], M. Mehmet[9,10], A. K. Mehta[19], E. Mejuto Villa[77,125], A. Melatos[110], G. Mendell[50], R. A. Mercer[24], L. Mereni[23], K. Merfeld[80], E. L. Merilh[50], J. D. Merritt[80], M. Merzougui[74], S. Meshkov[1], C. Messenger[54], C. Messick[177], R. Metzdorff[81], P. M. Meyers[110], F. Meylahn[9,10], A. Mhaske[3], A. Miani[126,127], H. Miao[13], I. Michaloliakos[32], C. Michel[23], H. Middleton[110], L. Milano[5,89], A. L. Miller[32,36,82], M. Millhouse[110], J. C. Mills[114], E. Milotti[27,178], M. C. Milovich-Goff[118], O. Minazzoli[74,179], Y. Minenkov[35], A. Mishkin[32], C. Mishra[180], T. Mistry[122], S. Mitra[3], V. P. Mitrofanov[68], G. Mitselmakher[32], R. Mittleman[55], G. Mo[55], K. Mogushi[96], S. R. P. Mohapatra[55], S. R. Mohite[24], M. Molina-Ruiz[149], M. Mondin[118], M. Montani[72,73], C. J. Moore[13], D. Moraru[50], F. Morawski[63], G. Moreno[50], S. Morisaki[92], B. Mours[181], C. M. Mow-Lowry[13], S. Mozzon[130], F. Muciaccia[36,82], Arunava Mukherjee[54], D. Mukherjee[132], S. Mukherjee[16], Subroto Mukherjee[120], N. Mukund[9,10], A. Mullavey[7], J. Munch[64], E. A. Muñiz[45], P. G. Murray[54], A. Nagar[98,139,182], I. Nardecchia[35,95], L. Naticchioni[36,82], R. K. Nayak[183], B. F. Neil[75], J. Neilson[77,125], G. Nelemans[40,184], T. J. N. Nelson[7], M. Nery[9,10], A. Neunzert[147], K. Y. Ng[55], S. Ng[64], C. Nguyen[28], P. Nguyen[80], D. Nichols[40,144], S. A. Nichols[2], S. Nissanke[40,144], F. Nocera[31], M. Noh[55], C. North[114], D. Nothard[185], L. K. Nuttall[130], J. Oberling[50], B. D. O'Brien[32], G. Oganesyan[17,18], G. H. Ogin[186], J. J. Oh[159], S. H. Oh[159], F. Ohme[9,10], H. Ohta[92], M. A. Okada[15], M. Oliver[111], C. Olivetto[31], P. Oppermann[9,10], Richard J. Oram[7], B. O'Reilly[7], R. G. Ormiston[47], L. F. Ortega[32], R. O'Shaughnessy[70], S. Ossokine[65], C. Osthelder[1], D. J. Ottaway[64], H. Overmier[7], B. J. Owen[94], A. E. Pace[132], G. Pagano[22,58], M. A. Page[75], G. Pagliaroli[17,18], A. Pai[140], S. A. Pai[67], J. R. Palamos[80], O. Palashov[156], C. Palomba[36], H. Pan[99], P. K. Panda[151], P. T. H. Pang[40], C. Pankow[14], F. Pannarale[36,82], B. C. Pant[67], F. Paoletti[22], A. Paoli[31], A. Parida[3], W. Parker[7,176], D. Pascucci[40,54], A. Pasqualetti[31], R. Passaquieti[22,58], D. Passuello[22], B. Patricelli[22,58], E. Payne[6], B. L. Pearlstone[54], T. C. Pechsiri[32], A. J. Pedersen[45], M. Pedraza[1], A. Pele[7], S. Penn[187], A. Perego[126,127], C. J. Perez[50], C. Périgois[37], A. Perreca[126,127], S. Perriès[106], J. Petermann[119], H. P. Pfeiffer[65],

M. Phelps[9,10], K. S. Phukon[3,40,169], O. J. Piccinni[36,82], M. Pichot[74], M. Piendibene[22,58], F. Piergiovanni[72,73], V. Pierro[77,125], G. Pillant[31], L. Pinard[23], I. M. Pinto[77,98,125], K. Piotrzkowski[83], M. Pirello[50], M. Pitkin[188], W. Plastino[172,173], R. Poggiani[22,58], D. Y. T. Pong[104], S. Ponrathnam[3], P. Popolizio[31], E. K. Porter[28], J. Powell[189], A. K. Prajapati[120], K. Prasai[57], R. Prasanna[151], G. Pratten[13], T. Prestegard[24], M. Principe[77,98,125], G. A. Prodi[126,127], L. Prokhorov[13], M. Punturo[44], P. Puppo[36], M. Pürrer[65], H. Qi[114], V. Quetschke[16], P. J. Quinonez[38], F. J. Raab[50], G. Raaijmakers[40,144], H. Radkins[50], N. Radulesco[74], P. Raffai[117], H. Rafferty[190], S. Raja[67], C. Rajan[67], B. Rajbhandari[94], M. Rakhmanov[16], K. E. Ramirez[16], A. Ramos-Buades[111], Javed Rana[3], K. Rao[14], P. Rapagnani[36,82], V. Raymond[114], M. Razzano[22,58], J. Read[29], T. Regimbau[37], L. Rei[66], S. Reid[25], D. H. Reitze[1,32], P. Rettegno[139,191], F. Ricci[36,82], C. J. Richardson[38], J. W. Richardson[1], P. M. Ricker[21], G. Riemenschneider[139,191], K. Riles[147], M. Rizzo[14], N. A. Robertson[1,54], F. Robinet[30], A. Rocchi[35], R. D. Rodriguez-Soto[38], L. Rolland[37], J. G. Rollins[1], V. J. Roma[80], M. Romanelli[79], R. Romano[4,5], C. L. Romel[50], I. M. Romero-Shaw[6], J. H. Romie[7], C. A. Rose[24], D. Rose[29], K. Rose[185], D. Rosińska[84], S. G. Rosofsky[21], M. P. Ross[171], S. Rowan[54], S. J. Rowlinson[13], P. K. Roy[16], Santosh Roy[3], Soumen Roy[192], P. Ruggi[31], G. Rutins[69], K. Ryan[50], S. Sachdev[132], T. Sadecki[50], M. Sakellariadou[153], O. S. Salafia[48,49,193], L. Salconi[31], M. Saleem[33], F. Salemi[126], A. Samajdar[40], E. J. Sanchez[1], L. E. Sanchez[1], N. Sanchis-Gual[194], J. R. Sanders[195], K. A. Santiago[39], E. Santos[74], N. Sarin[6], B. Sassolas[23], B. S. Sathyaprakash[114,132], O. Sauter[37], R. L. Savage[50], V. Savant[3], D. Sawant[140], S. Sayah[23], D. Schaetzl[1], P. Schale[80], M. Scheel[51], J. Scheuer[14], P. Schmidt[13], R. Schnabel[119], R. M. S. Schofield[80], A. Schönbeck[119], E. Schreiber[9,10], B. W. Schulte[9,10], B. F. Schutz[114], O. Schwarm[186], E. Schwartz[7], J. Scott[54], S. M. Scott[8], E. Seidel[21], D. Sellers[7], A. S. Sengupta[192], N. Sennett[65], D. Sentenac[31], V. Sequino[66], A. Sergeev[156], Y. Setyawati[9,10], D. A. Shaddock[8], T. Shaffer[50], M. S. Shahriar[14], A. Sharma[17,18], P. Sharma[67], P. Shawhan[86], H. Shen[21], M. Shikauchi[92], R. Shink[165], D. H. Shoemaker[55], D. M. Shoemaker[87], K. Shukla[149], S. ShyamSundar[67], K. Siellez[87], M. Sieniawska[63], D. Sigg[50], L. P. Singer[90], D. Singh[132], N. Singh[84], A. Singha[54], A. Singhal[17,36], A. M. Sintes[111], V. Sipala[128,129], V. Skliris[114], B. J. J. Slagmolen[8], T. J. Slaven-Blair[75], J. Smetana[13], J. R. Smith[29], R. J. E. Smith[6], S. Somala[196], E. J. Son[159], S. Soni[2], B. Sorazu[54], V. Sordini[106], F. Sorrentino[66], T. Souradeep[3], E. Sowell[94], A. P. Spencer[54], M. Spera[14,60,61], A. K. Srivastava[120], V. Srivastava[45], K. Staats[14], C. Stachie[74], M. Standke[9,10], D. A. Steer[28], J. Steinhoff[65], M. Steinke[9,10], J. Steinlechner[54,119], S. Steinlechner[119], D. Steinmeyer[9,10], S. Stevenson[189], D. Stocks[57], D. J. Stops[13], M. Stover[185], K. A. Strain[54], G. Stratta[73,197], A. Strunk[50], R. Sturani[198], A. L. Stuver[199], S. Sudhagar[3], V. Sudhir[55], T. Z. Summerscales[200], L. Sun[1], S. Sunil[120], A. Sur[63], J. Suresh[92], P. J. Sutton[114], B. L. Swinkels[40], M. J. Szczepańczyk[32], M. Tacca[40], S. C. Tait[54], C. Talbot[6], A. J. Tanasijczuk[83], D. B. Tanner[32], D. Tao[1], M. Tápai[141], A. Tapia[29], E. N. Tapia San Martin[40], J. D. Tasson[201], R. Taylor[1], R. Tenorio[111], L. Terkowski[119], M. P. Thirugnanasambandam[3], M. Thomas[7], P. Thomas[50], J. E. Thompson[114], S. R. Thondapu[67], K. A. Thorne[7], E. Thrane[6], C. L. Tinsman[6], T. R. Saravanan[3], Shubhanshu Tiwari[78,126,127], S. Tiwari[145], V. Tiwari[114], K. Toland[54], M. Tonelli[22,58], Z. Tornasi[54], A. Torres-Forné[65], C. I. Torrie[1], I. Tosta e Melo[128,129], D. Töyrä[8], E. A. Trail[2], F. Travasso[44,59], G. Traylor[7], M. C. Tringali[84], A. Tripathee[147], A. Trovato[28], R. J. Trudeau[1], K. W. Tsang[40], M. Tse[55], R. Tso[51], L. Tsukada[92], D. Tsuna[92], T. Tsutsui[92], M. Turconi[74], A. S. Ubhi[13], K. Ueno[92], D. Ugolini[190], C. S. Unnikrishnan[145], A. L. Urban[2], S. A. Usman[103], A. C. Utina[54], H. Vahlbruch[10], G. Vajente[1], G. Valdes[2], M. Valentini[126,127], N. van Bakel[40], M. van Beuzekom[40], J. F. J. van den Brand[40,85,150], C. Van Den Broeck[40,202], D. C. Vander-Hyde[45], L. van der Schaaf[40], J. V. Van Heijningen[75], A. A. van Veggel[54], M. Vardaro[40,169], V. Varma[51], S. Vass[1], M. Vasúth[56], A. Vecchio[13], G. Vedovato[61], J. Veitch[54], P. J. Veitch[64], K. Venkateswara[171], G. Venugopalan[1], D. Verkindt[37], D. Veske[34], F. Vetrano[72,73], A. Viceré[72,73], A. D. Viets[203], S. Vinciguerra[13], D. J. Vine[69], J.-Y. Vinet[74], S. Vitale[55], Francisco Hernandez Vivanco[6], T. Vo[45], H. Vocca[43,44], C. Vorvick[50], S. P. Vyatchanin[68], A. R. Wade[8], L. E. Wade[185], M. Wade[185], R. Walet[40], M. Walker[29], G. S. Wallace[25], L. Wallace[1], S. Walsh[24], J. Z. Wang[147], S. Wang[21], W. H. Wang[16], R. L. Ward[8], Z. A. Warden[38], J. Warner[50], M. Was[37], J. Watchi[112], B. Weaver[50], L.-W. Wei[9,10], M. Weinert[9,10], A. J. Weinstein[1], R. Weiss[55], F. Wellmann[9,10], L. Wen[75], P. Weßels[9,10], J. W. Westhouse[38], K. Wette[8], J. T. Whelan[70], B. F. Whiting[32], C. Whittle[55], D. M. Wilken[9,10], D. Williams[54], J. L. Willis[1], B. Willke[9,10], W. Winkler[9,10], C. C. Wipf[1], H. Wittel[9,10], G. Woan[54], J. Woehler[9,10], J. K. Wofford[70], C. Wong[104], J. L. Wright[54], D. S. Wu[9,10], D. M. Wysocki[70], L. Xiao[1], H. Yamamoto[1], L. Yang[133], Y. Yang[32], Z. Yang[47], M. J. Yap[8], M. Yazback[32], D. W. Yeeles[114], Hang Yu[55], Haocun Yu[55], S. H. R. Yuen[104], A. K. Zadrożny[16], A. Zadrożny[162], M. Zanolin[38], T. Zelenova[31], J.-P. Zendri[61], M. Zevin[14], J. Zhang[75], L. Zhang[1], T. Zhang[54], C. Zhao[75], G. Zhao[112], M. Zhou[14], Z. Zhou[14], X. J. Zhu[6], A. B. Zimmerman[177], M. E. Zucker[1,55], and J. Zweizig[1]

LIGO Scientific Collaboration and Virgo Collaboration

[1] LIGO, California Institute of Technology, Pasadena, CA 91125, USA
[2] Louisiana State University, Baton Rouge, LA 70803, USA
[3] Inter-University Centre for Astronomy and Astrophysics, Pune 411007, India
[4] Dipartimento di Farmacia, Università di Salerno, I-84084 Fisciano, Salerno, Italy
[5] INFN, Sezione di Napoli, Complesso Universitario di Monte S. Angelo, I-80126 Napoli, Italy
[6] OzGrav, School of Physics & Astronomy, Monash University, Clayton 3800, Victoria, Australia
[7] LIGO Livingston Observatory, Livingston, LA 70754, USA
[8] OzGrav, Australian National University, Canberra, Australian Capital Territory 0200, Australia
[9] Max Planck Institute for Gravitational Physics (Albert Einstein Institute), D-30167 Hannover, Germany
[10] Leibniz Universität Hannover, D-30167 Hannover, Germany
[11] Theoretisch-Physikalisches Institut, Friedrich-Schiller-Universität Jena, D-07743 Jena, Germany
[12] University of Cambridge, Cambridge CB2 1TN, UK
[13] University of Birmingham, Birmingham B15 2TT, UK
[14] Center for Interdisciplinary Exploration & Research in Astrophysics (CIERA), Northwestern University, Evanston, IL 60208, USA
[15] Instituto Nacional de Pesquisas Espaciais, 12227-010 São José dos Campos, São Paulo, Brazil

[16] The University of Texas Rio Grande Valley, Brownsville, TX 78520, USA
[17] Gran Sasso Science Institute (GSSI), I-67100 L'Aquila, Italy
[18] INFN, Laboratori Nazionali del Gran Sasso, I-67100 Assergi, Italy
[19] International Centre for Theoretical Sciences, Tata Institute of Fundamental Research, Bengaluru 560089, India
[20] University College Dublin, Dublin 4, Ireland
[21] NCSA, University of Illinois at Urbana-Champaign, Urbana, IL 61801, USA
[22] INFN, Sezione di Pisa, I-56127 Pisa, Italy
[23] Laboratoire des Matériaux Avancés (LMA), IP2I—UMR 5822, CNRS, Université de Lyon, F-69622 Villeurbanne, France
[24] University of Wisconsin-Milwaukee, Milwaukee, WI 53201, USA
[25] SUPA, University of Strathclyde, Glasgow G1 1XQ, UK
[26] Dipartimento di Matematica e Informatica, Università di Udine, I-33100 Udine, Italy
[27] INFN, Sezione di Trieste, I-34127 Trieste, Italy
[28] APC, AstroParticule et Cosmologie, Université Paris Diderot, CNRS/IN2P3, CEA/Irfu, Observatoire de Paris, Sorbonne Paris Cité, F-75205 Paris Cedex 13, France
[29] California State University Fullerton, Fullerton, CA 92831, USA
[30] LAL, Univ. Paris-Sud, CNRS/IN2P3, Université Paris-Saclay, F-91898 Orsay, France
[31] European Gravitational Observatory (EGO), I-56021 Cascina, Pisa, Italy
[32] University of Florida, Gainesville, FL 32611, USA
[33] Chennai Mathematical Institute, Chennai 603103, India
[34] Columbia University, New York, NY 10027, USA
[35] INFN, Sezione di Roma Tor Vergata, I-00133 Roma, Italy
[36] INFN, Sezione di Roma, I-00185 Roma, Italy
[37] Laboratoire d'Annecy de Physique des Particules (LAPP), Univ. Grenoble Alpes, Université Savoie Mont Blanc, CNRS/IN2P3, F-74941 Annecy, France
[38] Embry-Riddle Aeronautical University, Prescott, AZ 86301, USA
[39] Montclair State University, Montclair, NJ 07043, USA
[40] Nikhef, Science Park 105, 1098 XG Amsterdam, The Netherlands
[41] Korea Institute of Science and Technology Information, Daejeon 34141, Republic of Korea
[42] Christopher Newport University, Newport News, VA 23606, USA
[43] Università di Perugia, I-06123 Perugia, Italy
[44] INFN, Sezione di Perugia, I-06123 Perugia, Italy
[45] Syracuse University, Syracuse, NY 13244, USA
[46] Université de Liège, B-4000 Liège, Belgium
[47] University of Minnesota, Minneapolis, MN 55455, USA
[48] Università degli Studi di Milano-Bicocca, I-20126 Milano, Italy
[49] INFN, Sezione di Milano-Bicocca, I-20126 Milano, Italy
[50] LIGO Hanford Observatory, Richland, WA 99352, USA
[51] Caltech CaRT, Pasadena, CA 91125, USA
[52] Departament de Física Quàntica i Astrofísica, Institut de Ciències del Cosmos (ICCUB), Universitat de Barcelona (IEEC-UB), E-08028 Barcelona, Spain
[53] Dipartimento di Medicina, Chirurgia e Odontoiatria "Scuola Medica Salernitana," Università di Salerno, I-84081 Baronissi, Salerno, Italy
[54] SUPA, University of Glasgow, Glasgow G12 8QQ, UK
[55] LIGO, Massachusetts Institute of Technology, Cambridge, MA 02139, USA
[56] Wigner RCP, RMKI, H-1121 Budapest, Konkoly Thege Miklós út 29-33, Hungary
[57] Stanford University, Stanford, CA 94305, USA
[58] Università di Pisa, I-56127 Pisa, Italy
[59] Università di Camerino, Dipartimento di Fisica, I-62032 Camerino, Italy
[60] Università di Padova, Dipartimento di Fisica e Astronomia, I-35131 Padova, Italy
[61] INFN, Sezione di Padova, I-35131 Padova, Italy
[62] Montana State University, Bozeman, MT 59717, USA
[63] Nicolaus Copernicus Astronomical Center, Polish Academy of Sciences, 00-716, Warsaw, Poland
[64] OzGrav, University of Adelaide, Adelaide, South Australia 5005, Australia
[65] Max Planck Institute for Gravitational Physics (Albert Einstein Institute), D-14476 Potsdam-Golm, Germany
[66] INFN, Sezione di Genova, I-16146 Genova, Italy
[67] RRCAT, Indore, Madhya Pradesh 452013, India
[68] Faculty of Physics, Lomonosov Moscow State University, Moscow 119991, Russia
[69] SUPA, University of the West of Scotland, Paisley PA1 2BE, UK
[70] Rochester Institute of Technology, Rochester, NY 14623, USA
[71] Bar-Ilan University, Ramat Gan 5290002, Israel
[72] Università degli Studi di Urbino "Carlo Bo," I-61029 Urbino, Italy
[73] INFN, Sezione di Firenze, I-50019 Sesto Fiorentino, Firenze, Italy
[74] Artemis, Université Côte d'Azur, Observatoire Côte d'Azur, CNRS, CS 34229, F-06304 Nice Cedex 4, France
[75] OzGrav, University of Western Australia, Crawley, Western Australia 6009, Australia
[76] Dipartimento di Fisica "E.R. Caianiello," Università di Salerno, I-84084 Fisciano, Salerno, Italy
[77] INFN, Sezione di Napoli, Gruppo Collegato di Salerno, Complesso Universitario di Monte S. Angelo, I-80126 Napoli, Italy
[78] Physik-Institut, University of Zurich, Winterthurerstrasse 190, 8057 Zurich, Switzerland
[79] Univ Rennes, CNRS, Institut FOTON—UMR6082, F-3500 Rennes, France
[80] University of Oregon, Eugene, OR 97403, USA
[81] Laboratoire Kastler Brossel, Sorbonne Université, CNRS, ENS-Université PSL, Collège de France, F-75005 Paris, France
[82] Università di Roma "La Sapienza," I-00185 Roma, Italy
[83] Université catholique de Louvain, B-1348 Louvain-la-Neuve, Belgium
[84] Astronomical Observatory Warsaw University, 00-478 Warsaw, Poland
[85] VU University Amsterdam, 1081 HV Amsterdam, The Netherlands
[86] University of Maryland, College Park, MD 20742, USA
[87] School of Physics, Georgia Institute of Technology, Atlanta, GA 30332, USA
[88] Université de Lyon, Université Claude Bernard Lyon 1, CNRS, Institut Lumière Matière, F-69622 Villeurbanne, France
[89] Università di Napoli "Federico II," Complesso Universitario di Monte S.Angelo, I-80126 Napoli, Italy
[90] NASA Goddard Space Flight Center, Greenbelt, MD 20771, USA

[91] Dipartimento di Fisica, Università degli Studi di Genova, I-16146 Genova, Italy
[92] RESCEU, University of Tokyo, Tokyo, 113-0033, Japan
[93] Tsinghua University, Beijing 100084, People's Republic of China
[94] Texas Tech University, Lubbock, TX 79409, USA
[95] Università di Roma Tor Vergata, I-00133 Roma, Italy
[96] Missouri University of Science and Technology, Rolla, MO 65409, USA
[97] Departamento de Astronomía y Astrofísica, Universitat de València, E-46100 Burjassot, València, Spain
[98] Museo Storico della Fisica e Centro Studi e Ricerche "Enrico Fermi," I-00184 Roma, Italy
[99] National Tsing Hua University, Hsinchu City, 30013 Taiwan, Republic of China
[100] Charles Sturt University, Wagga Wagga, New South Wales 2678, Australia
[101] Physics and Astronomy Department, Stony Brook University, Stony Brook, NY 11794, USA
[102] Center for Computational Astrophysics, Flatiron Institute, 162 5th Avenue, New York, NY 10010, USA
[103] University of Chicago, Chicago, IL 60637, USA
[104] The Chinese University of Hong Kong, Shatin, NT, Hong Kong, People's Republic of China
[105] Dipartimento di Ingegneria Industriale (DIIN), Università di Salerno, I-84084 Fisciano, Salerno, Italy
[106] Institut de Physique des 2 Infinis de Lyon (IP2I) - UMR 5822, Université de Lyon, Université Claude Bernard, CNRS, F-69622 Villeurbanne, France
[107] Seoul National University, Seoul 08826, Republic of Korea
[108] Pusan National University, Busan 46241, Republic of Korea
[109] INAF, Osservatorio Astronomico di Padova, I-35122 Padova, Italy
[110] OzGrav, University of Melbourne, Parkville, Victoria 3010, Australia
[111] Universitat de les Illes Balears, IAC3—IEEC, E-07122 Palma de Mallorca, Spain
[112] Université Libre de Bruxelles, Brussels B-1050, Belgium
[113] Departamento de Matemáticas, Universitat de València, E-46100 Burjassot, València, Spain
[114] Cardiff University, Cardiff CF24 3AA, UK
[115] University of Rhode Island, Kingston, RI 02881, USA
[116] Bellevue College, Bellevue, WA 98007, USA
[117] MTA-ELTE Astrophysics Research Group, Institute of Physics, Eötvös University, Budapest 1117, Hungary
[118] California State University, Los Angeles, 5151 State University Dr, Los Angeles, CA 90032, USA
[119] Universität Hamburg, D-22761 Hamburg, Germany
[120] Institute for Plasma Research, Bhat, Gandhinagar 382428, India
[121] IGFAE, Campus Sur, Universidade de Santiago de Compostela, 15782 Spain
[122] The University of Sheffield, Sheffield S10 2TN, UK
[123] Dipartimento di Scienze Matematiche, Fisiche e Informatiche, Università di Parma, I-43124 Parma, Italy
[124] INFN, Sezione di Milano Bicocca, Gruppo Collegato di Parma, I-43124 Parma, Italy
[125] Dipartimento di Ingegneria, Università del Sannio, I-82100 Benevento, Italy
[126] Università di Trento, Dipartimento di Fisica, I-38123 Povo, Trento, Italy
[127] INFN, Trento Institute for Fundamental Physics and Applications, I-38123 Povo, Trento, Italy
[128] Università degli Studi di Sassari, I-07100 Sassari, Italy
[129] INFN, Laboratori Nazionali del Sud, I-95125 Catania, Italy
[130] University of Portsmouth, Portsmouth, PO1 3FX, UK
[131] West Virginia University, Morgantown, WV 26506, USA
[132] The Pennsylvania State University, University Park, PA 16802, USA
[133] Colorado State University, Fort Collins, CO 80523, USA
[134] Institute for Nuclear Research (Atomki), Hungarian Academy of Sciences, Bem tér 18/c, H-4026 Debrecen, Hungary
[135] CNR-SPIN, c/o Università di Salerno, I-84084 Fisciano, Salerno, Italy
[136] Scuola di Ingegneria, Università della Basilicata, I-85100 Potenza, Italy
[137] National Astronomical Observatory of Japan, 2-21-1 Osawa, Mitaka, Tokyo 181-8588, Japan
[138] Observatori Astronòmic, Universitat de València, E-46980 Paterna, València, Spain
[139] INFN Sezione di Torino, I-10125 Torino, Italy
[140] Indian Institute of Technology Bombay, Powai, Mumbai 400 076, India
[141] University of Szeged, Dóm tér 9, Szeged 6720, Hungary
[142] Delta Institute for Theoretical Physics, Science Park 904, 1090 GL Amsterdam, The Netherlands
[143] Lorentz Institute, Leiden University, P.O. Box 9506, Leiden 2300 RA, The Netherlands
[144] GRAPPA, Anton Pannekoek Institute for Astronomy and Institute for High-Energy Physics, University of Amsterdam, Science Park 904, 1098 XH Amsterdam, The Netherlands
[145] Tata Institute of Fundamental Research, Mumbai 400005, India
[146] INAF, Osservatorio Astronomico di Capodimonte, I-80131 Napoli, Italy
[147] University of Michigan, Ann Arbor, MI 48109, USA
[148] American University, Washington, D.C. 20016, USA
[149] University of California, Berkeley, CA 94720, USA
[150] Maastricht University, P.O. Box 616, 6200 MD Maastricht, The Netherlands
[151] Directorate of Construction, Services & Estate Management, Mumbai 400094 India
[152] University of Białystok, 15-424 Białystok, Poland
[153] King's College London, University of London, London WC2R 2LS, UK
[154] University of Southampton, Southampton SO17 1BJ, UK
[155] University of Washington Bothell, Bothell, WA 98011, USA
[156] Institute of Applied Physics, Nizhny Novgorod, 603950, Russia
[157] Ewha Womans University, Seoul 03760, Republic of Korea
[158] Inje University Gimhae, South Gyeongsang 50834, Republic of Korea
[159] National Institute for Mathematical Sciences, Daejeon 34047, Republic of Korea
[160] Ulsan National Institute of Science and Technology, Ulsan 44919, Republic of Korea
[161] Bard College, 30 Campus Rd, Annandale-On-Hudson, NY 12504, USA
[162] NCBJ, 05-400 Świerk-Otwock, Poland
[163] Institute of Mathematics, Polish Academy of Sciences, 00656 Warsaw, Poland
[164] Cornell University, Ithaca, NY 14850, USA
[165] Université de Montréal/Polytechnique, Montreal, Quebec H3T 1J4, Canada

[166] Lagrange, Université Côte d'Azur, Observatoire Côte d'Azur, CNRS, CS 34229, F-06304 Nice Cedex 4, France
[167] Hillsdale College, Hillsdale, MI 49242, USA
[168] Korea Astronomy and Space Science Institute, Daejeon 34055, Republic of Korea
[169] Institute for High-Energy Physics, University of Amsterdam, Science Park 904, 1098 XH Amsterdam, The Netherlands
[170] NASA Marshall Space Flight Center, Huntsville, AL 35811, USA
[171] University of Washington, Seattle, WA 98195, USA
[172] Dipartimento di Matematica e Fisica, Università degli Studi Roma Tre, I-00146 Roma, Italy
[173] INFN, Sezione di Roma Tre, I-00146 Roma, Italy
[174] ESPCI, CNRS, F-75005 Paris, France
[175] Center for Phononics and Thermal Energy Science, School of Physics Science and Engineering, Tongji University, 200092 Shanghai, People's Republic of China
[176] Southern University and A&M College, Baton Rouge, LA 70813, USA
[177] Department of Physics, University of Texas, Austin, TX 78712, USA
[178] Dipartimento di Fisica, Università di Trieste, I-34127 Trieste, Italy
[179] Centre Scientifique de Monaco, 8 quai Antoine Ier, MC-98000, Monaco
[180] Indian Institute of Technology Madras, Chennai 600036, India
[181] Université de Strasbourg, CNRS, IPHC UMR 7178, F-67000 Strasbourg, France
[182] Institut des Hautes Etudes Scientifiques, F-91440 Bures-sur-Yvette, France
[183] IISER-Kolkata, Mohanpur, West Bengal 741252, India
[184] Department of Astrophysics/IMAPP, Radboud University Nijmegen, P.O. Box 9010, 6500 GL Nijmegen, The Netherlands
[185] Kenyon College, Gambier, OH 43022, USA
[186] Whitman College, 345 Boyer Avenue, Walla Walla, WA 99362 USA
[187] Hobart and William Smith Colleges, Geneva, NY 14456, USA
[188] Department of Physics, Lancaster University, Lancaster, LA1 4 YB, UK
[189] OzGrav, Swinburne University of Technology, Hawthorn VIC 3122, Australia
[190] Trinity University, San Antonio, TX 78212, USA
[191] Dipartimento di Fisica, Università degli Studi di Torino, I-10125 Torino, Italy
[192] Indian Institute of Technology, Gandhinagar Ahmedabad Gujarat 382424, India
[193] INAF, Osservatorio Astronomico di Brera sede di Merate, I-23807 Merate, Lecco, Italy
[194] Centro de Astrofísica e Gravitação (CENTRA), Departamento de Física, Instituto Superior Técnico, Universidade de Lisboa, 1049-001 Lisboa, Portugal
[195] Marquette University, 11420 W. Clybourn Street, Milwaukee, WI 53233, USA
[196] Indian Institute of Technology Hyderabad, Sangareddy, Khandi, Telangana 502285, India
[197] INAF, Osservatorio di Astrofisica e Scienza dello Spazio, I-40129 Bologna, Italy
[198] International Institute of Physics, Universidade Federal do Rio Grande do Norte, Natal RN 59078-970, Brazil
[199] Villanova University, 800 Lancaster Avenue, Villanova, PA 19085, USA
[200] Andrews University, Berrien Springs, MI 49104, USA
[201] Carleton College, Northfield, MN 55057, USA
[202] Department of Physics, Utrecht University, 3584CC Utrecht, The Netherlands
[203] Concordia University Wisconsin, 2800 N Lake Shore Drive, Mequon, WI 53097, USA
Received 2020 May 2; revised 2020 May 21; accepted 2020 May 22; published 2020 June 23

Abstract

We report the observation of a compact binary coalescence involving a 22.2–24.3 $M_\odot$ black hole and a compact object with a mass of 2.50–2.67 $M_\odot$ (all measurements quoted at the 90% credible level). The gravitational-wave signal, GW190814, was observed during LIGO's and Virgo's third observing run on 2019 August 14 at 21:10:39 UTC and has a signal-to-noise ratio of 25 in the three-detector network. The source was localized to 18.5 deg^2 at a distance of 241^{+41}_{-45} Mpc; no electromagnetic counterpart has been confirmed to date. The source has the most unequal mass ratio yet measured with gravitational waves, $0.112^{+0.008}_{-0.009}$, and its secondary component is either the lightest black hole or the heaviest neutron star ever discovered in a double compact-object system. The dimensionless spin of the primary black hole is tightly constrained to $\leqslant 0.07$. Tests of general relativity reveal no measurable deviations from the theory, and its prediction of higher-multipole emission is confirmed at high confidence. We estimate a merger rate density of 1–23 Gpc^{-3} yr^{-1} for the new class of binary coalescence sources that GW190814 represents. Astrophysical models predict that binaries with mass ratios similar to this event can form through several channels, but are unlikely to have formed in globular clusters. However, the combination of mass ratio, component masses, and the inferred merger rate for this event challenges all current models of the formation and mass distribution of compact-object binaries.

Unified Astronomy Thesaurus concepts: Gravitational wave astronomy (675); Gravitational wave sources (677); Astrophysical black holes (98); Compact binary stars (283); Gravitational waves (678); Gravitational wave detectors (676)

1. Introduction

The first two observing runs (O1 and O2) with Advanced LIGO (Aasi et al. 2015) and Advanced Virgo (Acernese et al. 2015) opened up the field of gravitational-wave astrophysics with the detection of the first binary black hole (BBH) coalescence signal, GW150914 (Abbott et al. 2016a). Another nine such events (Abbott et al. 2016b, 2019a) were discovered by the LIGO Scientific and Virgo Collaborations (LVC) during this period, and additional events were reported by independent groups (Venumadhav et al. 2020; Zackay et al. 2019a, 2019b; Nitz

et al. 2020). The first binary neutron star (BNS) coalescence signal, GW170817, was discovered during the second of these observing campaigns (Abbott et al. 2017a, 2019b). It proved to be a multmessenger source with emission across the electromagnetic spectrum (Abbott et al. 2017b), with implications for the origin of short gamma-ray bursts (Abbott et al. 2017c), the formation of heavy elements (Abbott et al. 2017d; Chornock et al. 2017; Tanvir et al. 2017; Rosswog et al. 2018; Kasliwal et al. 2019; Watson et al. 2019), cosmology (Abbott et al. 2017e, 2019c), and fundamental physics (Abbott et al. 2017c, 2019d).

The first six months of the third observing run (O3) were completed between 2019 April 1 and September 30. The LVC recently reported on the discovery of GW190425, the coalescence signal of what is most likely a BNS with unusually large chirp mass and total mass compared to the Galactic BNSs known from radio pulsar observations (Abbott et al. 2020a). Another discovery from O3 is that of GW190412, the first BBH coalescence with an unequivocally unequal mass ratio $q = m_2/m_1$ of $0.28^{+0.12}_{-0.06}$ (all measurements are reported as symmetric 90% credible intervals around the median of the marginalized posterior distribution, unless otherwise specified). It is also the first event for which higher-multipole gravitational radiation was detected with high significance (Abbott et al. 2020d).

Here we report on another O3 detection, GW190814, the signal of a compact binary coalescence with the most unequal mass ratio yet measured with gravitational waves: $q = 0.112^{+0.008}_{-0.009}$. The signal was first identified in data from two detectors, LIGO Livingston and Virgo, on 2019 August 14, 21:11:00 UTC. Subsequent analysis of data from the full three-detector network revealed a merger signal with signal-to-noise ratio (S/N) of $\simeq$25.

The primary component of GW190814 is conclusively a black hole (BH) with mass $m_1 = 23.2^{+1.1}_{-1.0}\,M_\odot$. Its dimensionless spin magnitude is constrained to $\chi_1 \leqslant 0.07$. The nature of the $2.59^{+0.08}_{-0.09}$ $M_\odot$ secondary component is unclear. The lack of measurable tidal deformations and the absence of an electromagnetic counterpart are consistent with either a neutron star (NS) or a BH given the event's asymmetric masses and distance of 241^{+41}_{-45} Mpc. However, we show here that comparisons with the maximum NS mass predicted by studies of GW170817's remnant, by current knowledge of the NS equation of state, and by electromagnetic observations of NSs in binary systems indicate that the secondary is likely too heavy to be an NS. Either way, this is an unprecedented source because the secondary's well-constrained mass of 2.50–2.67 $M_\odot$ makes it either the lightest BH or the heaviest NS ever observed in a double compact-object system.

As in the case of GW190412, we are able to measure the presence of higher multipoles in the gravitational radiation, and a set of tests of general relativity with the signal reveal no deviations from the theory. Treating this event as a new class of compact binary coalescences, we estimate a merger rate density of 1–23 $\mathrm{Gpc}^{-3}\,\mathrm{yr}^{-1}$ for GW190814-like events. Forming coalescing compact binaries with this unusual combination of masses at such a rate challenges our current understanding of astrophysical models.

We report on the status of the detector network and the specifics of the detection in Sections 2 and 3. In Section 4, we estimate physical source properties with a set of waveform models, and we assess statistical and systematic uncertainties. Tests of general relativity are described in Section 5. In Section 6, we calculate the merger rate density and discuss implications for the nature of the secondary component, compact binary formation, and cosmology. Section 7 summarizes our findings.

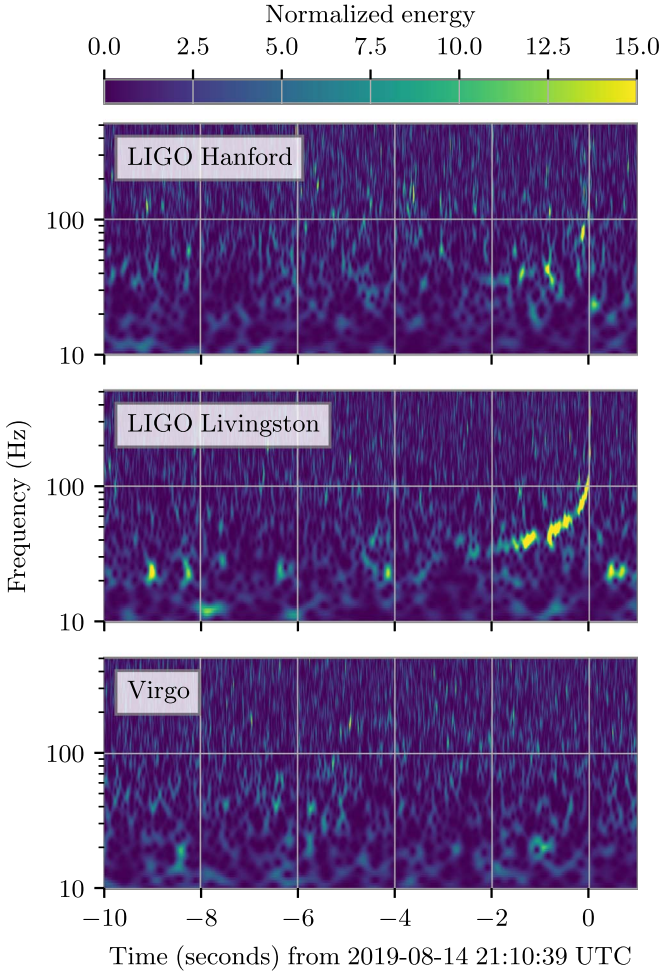

Figure 1. Time–frequency representations (Chatterji et al. 2004) of data containing GW190814, observed by LIGO Hanford (top), LIGO Livingston (middle), and Virgo (bottom). Times are shown relative to 2019 August 14, 21:10:39 UTC. Each detector's data are whitened by their respective noise amplitude spectral density and a Q-transform is calculated. The colorbar displays the normalized energy reported by the Q-transform at each frequency. These plots are not used in our detection procedure and are for visualization purposes only.

2. Detector Network

At the time of GW190814, LIGO Hanford, LIGO Livingston, and Virgo were operating with typical O3 sensitivities (Abbott et al. 2020a). Although LIGO Hanford was in a stable operating configuration at the time of GW190814, the detector was not in observing mode due to a routine procedure to minimize angular noise coupling to the strain measurement (Kasprzack & Yu 2017). This same procedure took place at LIGO Hanford around the time of GW170608; we refer the reader to Abbott et al. (2017f) for details of this procedure. Within a 5 minute window around GW190814, this procedure was not taking place; therefore, LIGO Hanford data for GW190814 are usable in the nominal range of analyzed frequencies. A time–frequency representation (Chatterji et al. 2004) of the data from all three detectors around the time of the signal is shown in Figure 1.

We used validation procedures similar to those used to vet previous gravitational-wave events (Abbott et al. 2016c, 2019a). Overall we found no evidence that instrumental or environmental disturbances (Effler et al. 2015) could account for GW190814. However, we did identify low-frequency transient noise due to scattered light at LIGO Livingston, a common source of noise in

all three interferometers (Nuttall 2018). Scattered light features in the strain data are produced when a small fraction of the main laser beam reflects off a moving surface and is phase modulated before recombining with the main beam. This recombination can result in excess noise with the morphology of arches in the time–frequency plane; the frequency of this noise is determined by the velocity of the moving surface (Accadia et al. 2010). Thunderstorms near LIGO Livingston around the time of GW190814 resulted in acoustic noise coupling to the detector and caused features in the strain data associated with scattered light (Abbott et al. 2019a). In this instance, this form of noise affects frequencies up to 30 Hz from roughly 22 s to 8 s before and 0.2 s to 1.5 s after the detected time of GW190814, as seen in the middle panel of Figure 1. Since this noise could bias the estimation of GW190814's source parameters, we used a starting frequency of 30 Hz to analyze LIGO Livingston data. Virgo was operating nominally and there are no quality issues in the Virgo data.

The LIGO and Virgo detectors are calibrated by photon pressure from modulated auxiliary lasers inducing test-mass motion (Karki et al. 2016; Acernese et al. 2018; Viets et al. 2018). Over the frequency range of 20–2048 Hz, the maximum 1σ calibration uncertainties for strain data used in the analysis of GW190814 were 6% in amplitude and 4 deg in phase for LIGO data, and 5% in amplitude and 7 deg in phase for Virgo data. These calibration uncertainties are propagated into the parameter estimation reported in Section 4 via marginalization.

3. Detection

3.1. Low-latency Identification of a Candidate Event

GW190814 was first identified on 2019 August 14, 21:11:00 UTC as a loud two-detector event in LIGO Livingston and Virgo data (S/N 21.4 and 4.3) by the low-latency GstLAL matched-filtering search pipeline for coalescing binaries (Cannon et al. 2012; Privitera et al. 2014; Messick et al. 2017; Sachdev et al. 2019; Hanna et al. 2020). Matched-filtering searches use banks (Sathyaprakash & Dhurandhar 1991; Blanchet et al. 1995; Owen 1996; Owen & Sathyaprakash 1999; Damour et al. 2001; Blanchet et al. 2005; Cokelaer 2007; Harry et al. 2009; Brown et al. 2013; Ajith et al. 2014; Harry et al. 2014; Capano et al. 2016b; Roy et al. 2017, 2019a; Indik et al. 2018) of modeled gravitational waveforms (Buonanno & Damour 1999; Arun et al. 2009; Blanchet 2014; Bohé et al. 2017; Pürrer 2016) as filter templates. A Notice was issued through NASA's Gamma-ray Coordinates Network (GCN) 20 minutes later (LIGO Scientific Collaboration & Virgo Collaboration 2019a) with a two-detector source localization computed using the rapid Bayesian algorithm BAYESTAR (Singer & Price 2016) that is shown in Figure 2. The event was initially classified as "MassGap"(Kapadia et al. 2020; LIGO Scientific Collaboration & Virgo Collaboration 2019b), implying that at least one of the binary merger components was found to have a mass between 3 and 5 $M_\odot$ in the low-latency analyses.

Other low-latency searches, including the matched-filtering based MBTA (Adams et al. 2016) and PyCBC (Nitz et al. 2017, 2018, 2019; Usman et al. 2016) pipelines, could not detect the event at the time as its S/N in Virgo data was below their single-detector detection thresholds. Test versions of MBTA and the additional matched-filtering pipeline SPIIR (Hooper et al. 2012; Liu et al. 2012; Guo et al. 2018) operating with a lower S/N threshold also identified the event with consistent attributes.

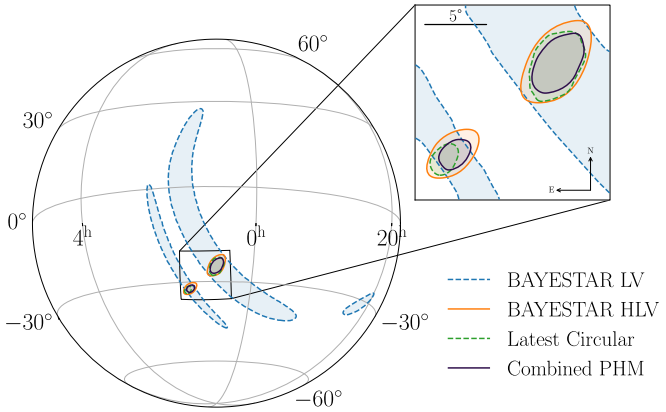

Figure 2. Posterior distributions for the sky location of GW190814. The contours show the 90% credible interval for a LIGO Livingston–Virgo (blue) and LIGO Hanford–LIGO Livingston–Virgo (orange) detector network based on the rapid localization algorithm BAYESTAR (Singer & Price 2016). The sky localization circulated 13.5 hr after the event, based on a LIGO Hanford–LIGO Livingston–Virgo analysis with the LALINFERENCE stochastic sampling software (Veitch et al. 2015), is shown in green. The purple contour indicates the final sky localization as presented in this paper, which constrains the source to within 18.5 deg^2 at 90% probability.

Shortly thereafter, reanalyses including LIGO Hanford data were performed using GstLAL and PyCBC. A coincident gravitational-wave signal was identified in all three detectors by both searches, with S/N 21.6 in LIGO Livingston, 10.6 in LIGO Hanford, and 4.5 in Virgo data (as measured by GstLAL, consistent with S/Ns reported by PyCBC). Results of these three-detector analyses were reported in a GCN Circular within 2.3 hr of the time of the event (LIGO Scientific Collaboration & Virgo Collaboration 2019c, 2019d), providing a three-detector localization (Singer & Price 2016) constraining the distance to 220–330 Mpc and the sky area to 38 deg^2 at the 90% credible level. Another GCN Circular (LIGO Scientific Collaboration & Virgo Collaboration 2019e) sent 13.5 hours after the event updated the source localization to a distance of 215–320 Mpc, the sky area to 23 deg^2, and the source classification to "NSBH" (Kapadia et al. 2020; LIGO Scientific Collaboration & Virgo Collaboration 2019b), indicating that the secondary had a mass below 3 $M_\odot$. These updated sky localizations are also shown in Figure 2. The two disjoint sky localizations arise because the low S/N in the Virgo detector (4.5) means that the data are consistent with two different signal arrival times in that detector.

3.2. Multimessenger Follow-up

Several external groups performed multimessenger follow-up of the source with observations across the electromagnetic spectrum (e.g., Dobie et al. 2019; Gomez et al. 2019; Lipunov et al. 2019; Ackley et al. 2020; Antier et al. 2020; Andreoni et al. 2020; Watson et al. 2020; Vieira et al. 2020) and with neutrino observations (e.g., Ageron et al. 2019; The IceCube Collaboration 2019). No counterpart candidates were reported. The nondetection is consistent with the source's highly unequal mass ratio and low primary spin (LIGO Scientific Collaboration & Virgo Collaboration 2019d, 2019e; Fernández et al. 2020; Morgan et al. 2020). Tentative constraints placed by multi-messenger studies on the properties of the system, such as the ejecta mass and maximum primary spin (Ackley et al. 2020; Andreoni et al. 2020; Coughlin et al. 2020; Kawaguchi et al. 2020) or the circum-merger density (Dobie et al. 2019) assuming

a neutron star–black hole (NSBH) source, may need to be revisited in light of the updated source parameters we present in Section 4.1.

3.3. Significance

The significance of GW190814 was estimated by follow-up searches using improved calibration and refined data-quality information that are not available in low latency. They also used longer stretches of data for better precision (Abbott et al. 2016b, 2016c). With LIGO Hanford data being usable but not in nominal observing mode at the time of GW190814, we used only data from the LIGO Livingston and Virgo detectors for significance estimation. GW190814 was identified as a confident detection in analyses of detector data collected over the period from 2019 August 7 to August 15 by the two independent matched-filtering searches GstLAL and PyCBC, with S/N values consistent with the low-latency analyses. The production version of PyCBC for O3 estimates significance only for events that are coincident in the LIGO Hanford and LIGO Livingston detectors, and therefore an extended version (Davies et al. 2020) was used for GW190814 in order to enable the use of Virgo data in significance estimation.

GstLAL and PyCBC use different techniques for estimating the noise background and methods of ranking gravitational-wave candidates. Both use results from searches over non-time-coincident data to improve their noise background estimation (Privitera et al. 2014; Messick et al. 2017; Usman et al. 2016). Using data from the first six months of O3 and including all events during this period in the estimation of noise background, GstLAL estimated a false-alarm rate (FAR) of 1 in 1.3×10^3 yr for GW190814. Using data from the 8 day period surrounding GW190814 and including this and all quieter events during this period in noise background estimation, the extended PyCBC pipeline (Davies et al. 2020) estimated an FAR for the event of 1 in 8.1 yr. The higher FAR estimate from PyCBC can be attributed to the event being identified by the pipeline as being quieter than multiple noise events in Virgo data. As PyCBC estimates background statistics using noncoincident data from both detectors, these louder noise events in Virgo data can form chance coincidences with the signal in LIGO Livingston data and elevate the noise background estimate for coincident events, especially when considering shorter data periods. All estimated background events that were ranked higher than GW190814 by PyCBC were indeed confirmed to be coincidences of the candidate event itself in LIGO Livingston with random noise events in Virgo. The stated background estimates are therefore conservative (Capano et al. 2016a). We also estimate the background excluding the candidate from the calculation, a procedure that yields a mean-unbiased estimation of the distribution of noise events (Abbott et al. 2016d; Capano et al. 2016a). In this case, with GstLAL we found an FAR of <1 in 10^5 yr while with PyCBC we found an FAR of <1 in 4.2×10^4 yr. With both pipelines identifying GW190814 as more significant than any event in the background, the FARs assigned are upper bounds.

When data from LIGO Hanford were included, GW190814 was also identified by the unmodeled coherent WaveBurst (cWB) search that targets generic gravitational-wave transients with increasing frequency over time without relying on waveform models (Klimenko et al. 2008, 2016; Abbott et al. 2016e). We found an FAR of <1 in 10^3 yr of observing time against the noise background from LIGO Hanford and LIGO Livingston data, consistent with the other searches.

4. Properties of GW190814

We infer the physical properties of GW190814 using a coherent Bayesian analysis of the data from LIGO Livingston, LIGO Hanford, and Virgo following the methodology described in Appendix B of Abbott et al. (2019a). Results presented here are obtained using 16 s of data around the time of detection. We use a low-frequency cutoff of 20 Hz for LIGO Hanford and Virgo and 30 Hz for LIGO Livingston for the likelihood evaluations, and we choose uninformative and wide priors, as defined in Appendix B.1 of Abbott et al. (2019a). The LALInference stochastic sampling software (Veitch et al. 2015) is the primary tool used to sample the posterior distribution. A parallelized version of the parameter estimation software BILBY (PBILBY; Ashton et al. 2019; Smith & Ashton 2019) is used for computationally expensive signal models. The power spectral density used in the likelihood calculations is a fair draw estimate calculated with BayesWave (Cornish & Littenberg 2015; Littenberg & Cornish 2015).

This signal is analyzed under two different assumptions: that it represents a BBH, or that it represents an NSBH. For the BBH analyses, two different waveform families are used, one based on the effective-one-body approach (EOBNR; Bohé et al. 2017; Babak et al. 2017; Cotesta et al. 2018; Ossokine et al. 2020) and the other on a phenomenological approach (Phenom; Husa et al. 2016; Khan et al. 2016, 2019, 2020; London et al. 2018).

For the NSBH analyses, we use BBH waveform models augmented with tidal effects (Matas et al. 2020; Thompson et al. 2020a). Systematic uncertainties due to waveform modeling are expected to be subdominant compared to statistical errors (Huang et al. 2020). When sampling the parameter space with the SEOBNRv4_ROM_NRTidalv2_NSBH (Matas et al. 2020) and IMRPhenomNSBH (Thompson et al. 2020a) waveform models, we obtained posterior distributions for the secondary component's tidal deformability Λ_2 that are uninformative relative to a uniform prior in $\Lambda_2 \in [0, 3000]$. The absence of a measurable tidal signature is consistent with the highly unequal mass ratio (Foucart et al. 2013; Kumar et al. 2017) and with the relatively large secondary mass (Flanagan & Hinderer 2008). The large asymmetry in the masses implies that the binary will merge before the neutron star is tidally disrupted for any expected NS equation of state (Foucart et al. 2013). Given that the signal carries no discernible information about matter effects, here we present quantitative results only from BBH waveform models.

Our primary analyses include the effect of subdominant multipole moments in precessing waveform template models (PHM): IMRPhenomPv3HM (Phenom PHM; Khan et al. 2019, 2020) from the phenomenological family and SEOBNRv4PHM (EOBNR PHM; Babak et al. 2017; Ossokine et al. 2020) from the EOBNR family.[204] Analyses that assume the spins are aligned with the orbital angular momentum were also performed, either including (Phenom/EOBNR HM) or excluding (Phenom/EOBNR) the effect of subdominant multipole moments.

4.1. Properties

From the ∼300 observed cycles above 20 Hz, we are able to tightly constrain the source properties of GW190814. Our analysis shows that GW190814's source is a binary with an

[204] In the coprecessing frame the EOBNR model includes the $(l, m) = (2, \pm2)$, $(2, \pm1)$, $(3, \pm3)$, $(4, \pm4)$, and $(5, \pm5)$ multipoles, and the Phenom model includes the $(2, \pm2)$, $(2, \pm1)$, $(3, \pm3)$, $(3, \pm2)$, $(4, \pm4)$, and $(4, \pm3)$ multipoles.

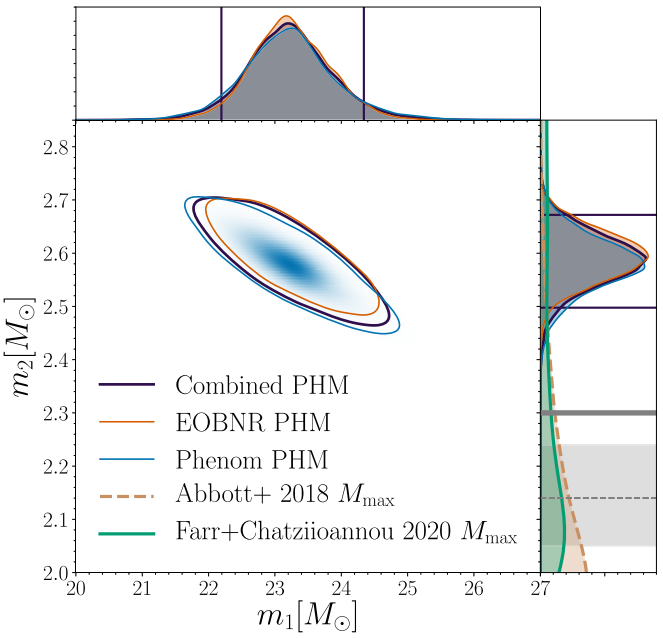

Figure 3. Posterior distribution of the primary and secondary source masses for two waveform models that include precession and subdominant multipole moments. The posterior distribution resulting from combining their samples is also shown. Each contour, as well as the colored horizontal and vertical lines, shows the 90% credible intervals. The right panel compares m_2 to predictions for the maximum NS mass, $M_{\rm max}$ (see Section 6). The posterior distribution for $M_{\rm max}$ from the spectral equation of state analysis of GW170817 (Abbott et al. 2018) is shown in orange, and the empirical $M_{\rm max}$ distribution from the population model of Farr & Chatziioannou (2020) is shown in green. The gray dashed line and shading represent the measured mass of the heaviest pulsar in the Galaxy (median and 68% confidence interval; Cromartie et al. 2019). The solid gray band at $2.3\,M_\odot$ is the upper bound on $M_{\rm max}$ from studies of GW170817's merger remnant.

unequal mass ratio $q = 0.112^{+0.008}_{-0.009}$, with individual source masses $m_1 = 23.2^{+1.1}_{-1.0}\,M_\odot$ and $m_2 = 2.59^{+0.08}_{-0.09}\,M_\odot$, as shown in Figure 3. A summary of the inferred source properties is given in Table 1. We assume a standard flat ΛCDM cosmology with Hubble constant $H_0 = 67.9\ \ {\rm km\,s^{-1}\,Mpc^{-1}}$ (Ade et al. 2016).

We report detailed results obtained from the two precessing BBH signal models including subdominant multipole moments: Phenom PHM and EOBNR PHM. In order to compare the template models, we compute their Bayes factor ($\log_{10}\mathcal{B}$). We find no significant evidence that one waveform family is preferred over the other as the Bayes factor between Phenom PHM and EOBNR PHM is $\log_{10}\mathcal{B} \simeq 1.0$. As a result, we combine the posterior samples with equal weight, in effect marginalizing over a discrete set of signal models with a uniform probability. This is shown in the last column of Table 1, and we refer to these values throughout the paper unless stated otherwise.

We find that the secondary mass lies in the range of 2.50–2.67 $M_\odot$. This inferred secondary mass exceeds the bounds of the primary component in GW190425 (1.61–2.52 $M_\odot$; Abbott et al. 2020a) and the most massive known pulsar in the Galaxy: $2.14^{+0.10}_{-0.09}\,M_\odot$ at 68.3% credible interval (Cromartie et al. 2019). Furthermore, the secondary is more massive than bounds on the maximum NS mass from studies of the remnant of GW170817, and from theoretical (Abbott et al. 2018) and observational estimates (Farr & Chatziioannou 2020). The inferred secondary mass is comparable to the putative BH remnant mass of GW170817 (Abbott et al. 2019b).

The primary object is identified as a BH based on its measured mass of $23.2^{+1.1}_{-1.0}\,M_\odot$. Due to accurately observing the frequency evolution over a long inspiral, the chirp mass is well constrained to $6.09^{+0.06}_{-0.06}\,M_\odot$. The inferred mass ratio $q = 0.112^{+0.008}_{-0.009}$ makes GW190814 only the second gravitational-wave observation with a significantly unequal mass ratio (Abbott et al. 2019a, 2020d).

Given that this system is in a region of the parameter space that has not been explored via gravitational-wave emission previously, we test possible waveform systematics by comparing the Phenom and EOB waveform families. Differences in the inferred secondary mass are shown in Figure 4. The results indicate that the inferred secondary mass is robust to possible waveform systematics, with good agreement between the Phenom PHM and EOBNR PHM signal models. Signal models that exclude higher multipoles or precession do not constrain the secondary mass as well.

The time delay of a signal across a network of gravitational wave detectors, together with the relative amplitude and phase at each detector, allows us to measure the location of the GW source on the sky (Abbott et al. 2020b). We localize GW190814's source to within 18.5 $\deg^2$ at 90% probability, as shown in Figure 2. This is comparable to the localization of GW170817 (Abbott et al. 2017a, 2019a).

Spins are a fundamental property of BHs. Their magnitude and orientation carry information regarding the evolution history of the binary. The effective inspiral spin parameter $\chi_{\rm eff}$ (Damour 2001; Racine 2008; Santamaría et al. 2010; Ajith et al. 2011) contains information about the spin components that are perpendicular to the orbital plane. We infer that $\chi_{\rm eff} = -0.002^{+0.060}_{-0.061}$. The tight constraints are consistent with being able to measure the phase evolution from the long inspiral.

Orbital precession occurs when there is a significant spin component in the orbital plane of the binary (Apostolatos et al. 1994). We parameterize precession by the effective precession spin parameter $0 \leqslant \chi_{\rm p} \leqslant 1$ (Schmidt et al. 2015). This effect is difficult to measure for face-on and face-off systems (Apostolatos et al. 1994; Buonanno et al. 2003; Vitale et al. 2014, 2017; Fairhurst et al. 2019a, 2019b). GW190814 constrains the inclination of the binary to be $\Theta = 0.8^{+0.3}_{-0.2}$ rad. Since the system is neither face-on nor face-off, we are able to put strong constraints on the precession of the system: $\chi_{\rm p} = 0.04^{+0.04}_{-0.03}$. This is both the strongest constraint on the amount of precession for any gravitational-wave detection to date, and the first gravitational-wave measurement that conclusively measures near-zero precession (Abbott et al. 2019a, 2020a, 2020d).

By computing the Bayes factor between a precessing and nonprecessing signal model ($\log_{10}\mathcal{B} \sim 0.5$ in favor of precession), we find inconclusive evidence for in-plane spin. This is consistent with the inferred power from precession S/N $\rho_{\rm p}$ (Fairhurst et al. 2019a, 2019b), whose recovered distribution resembles that expected in the absence of any precession in the signal; see Figure 5. The $\rho_{\rm p}$ calculation assumes a signal dominated by the $\ell = 2$ mode; however, we have verified that the contribution of higher harmonics to the measurement of spin precession is subdominant by a factor of 5. The data are therefore consistent with the signal from a nonprecessing system.

Figure 4 shows that signal models including spin-precession effects give tighter constraints on the secondary mass compared to their nonprecessing equivalents. Signal models that include spin-precession effects can constrain $\chi_{\rm p}$, whereas nonprecessing signal models cannot provide information on in-plane spin

Table 1
Source Properties of GW190814: We Report the Median Values Along with the Symmetric 90% Credible Intervals for the SEOBNRv4PHM (EOBNR PHM) and IMRPHENOMPV3HM (PHENOM PHM) Waveform Models

	EOBNR PHM	Phenom PHM	Combined
Primary mass $m_1/M_\odot$	$23.2^{+1.0}_{-0.9}$	$23.2^{+1.3}_{-1.1}$	$23.2^{+1.1}_{-1.0}$
Secondary mass $m_2/M_\odot$	$2.59^{+0.08}_{-0.08}$	$2.58^{+0.09}_{-0.10}$	$2.59^{+0.08}_{-0.09}$
Mass ratio q	$0.112^{+0.008}_{-0.008}$	$0.111^{+0.009}_{-0.010}$	$0.112^{+0.008}_{-0.009}$
Chirp mass $\mathcal{M}/M_\odot$	$6.10^{+0.06}_{-0.05}$	$6.08^{+0.06}_{-0.05}$	$6.09^{+0.06}_{-0.06}$
Total mass $M/M_\odot$	$25.8^{+0.9}_{-0.8}$	$25.8^{+1.2}_{-1.0}$	$25.8^{+1.0}_{-0.9}$
Final mass $M_f/M_\odot$	$25.6^{+1.0}_{-0.8}$	$25.5^{+1.2}_{-1.0}$	$25.6^{+1.1}_{-0.9}$
Upper bound on primary spin magnitude χ_1	0.06	0.08	0.07
Effective inspiral spin parameter $\chi_{\rm eff}$	$0.001^{+0.059}_{-0.056}$	$-0.005^{+0.061}_{-0.065}$	$-0.002^{+0.060}_{-0.061}$
Upper bound on effective precession parameter $\chi_{\rm p}$	0.07	0.07	0.07
Final spin χ_f	$0.28^{+0.02}_{-0.02}$	$0.28^{+0.02}_{-0.03}$	$0.28^{+0.02}_{-0.02}$
Luminosity distance D_L/Mpc	235^{+40}_{-45}	249^{+39}_{-43}	241^{+41}_{-45}
Source redshift z	$0.051^{+0.008}_{-0.009}$	$0.054^{+0.008}_{-0.009}$	$0.053^{+0.009}_{-0.010}$
Inclination angle Θ/rad	$0.9^{+0.3}_{-0.2}$	$0.8^{+0.2}_{-0.2}$	$0.8^{+0.3}_{-0.2}$
Signal-to-noise ratio in LIGO Hanford ρ_H	$10.6^{+0.1}_{-0.1}$	$10.7^{+0.1}_{-0.2}$	$10.7^{+0.1}_{-0.2}$
Signal-to-noise ratio in LIGO Livingston ρ_L	$22.21^{+0.09}_{-0.15}$	$22.16^{+0.09}_{-0.17}$	$22.18^{+0.10}_{-0.17}$
Signal-to-noise ratio in Virgo ρ_V	$4.3^{+0.2}_{-0.5}$	$4.1^{+0.2}_{-0.6}$	$4.2^{+0.2}_{-0.6}$
Network Signal-to-noise ratio ρ_{HLV}	$25.0^{+0.1}_{-0.2}$	$24.9^{+0.1}_{-0.2}$	$25.0^{+0.1}_{-0.2}$

Note. The primary spin magnitude and the effective precession is given as the 90% upper limit. The inclination angle is folded to $[0, \pi/2]$. The last column is the result of combining the posteriors of each model with equal weight. The sky location of GW190814 is shown in Figure 2.

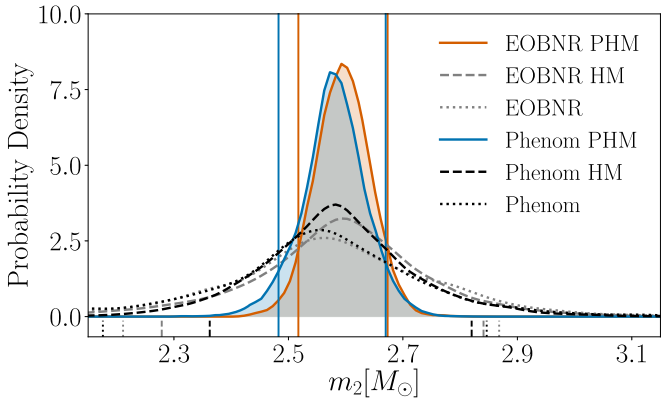

Figure 4. Marginalized posterior distribution for the secondary mass obtained using a suite of waveform models. The vertical lines indicate the 90% credible bounds for each waveform model. The labels Phenom/EOBNR PHM (generic spin directions + higher multipoles), Phenom/EOBNR HM (aligned-spin + higher multipoles), and Phenom/EOBNR (aligned-spin, quadrupole only) indicate the different physical content in each of the waveform models.

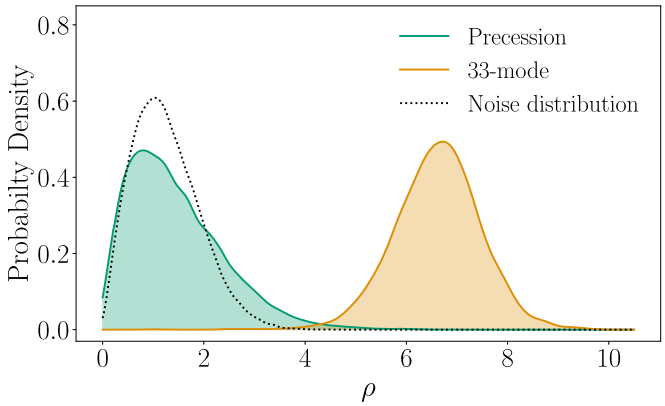

Figure 5. Posterior distributions for the precessing S/N, ρ_p (green) and the optimal S/N in the (3, 3) subdominant multipole moment, ρ (orange). The gray dotted line shows the expected distribution for Gaussian noise.

components. In all analyses, we assume a prior equivalent to spin orientations being isotropically distributed. We find that the data are inconsistent with large χ_p and consistent with any secondary spin. Therefore, for precessing signal models the allowed q–$\chi_{\rm eff}$ parameter space is restricted, which helps to break the degeneracy (Poisson & Will 1995; Baird et al. 2013; Farr et al. 2016; Ng et al. 2018). Consequently, the extra information from constraining χ_p to small values enables a more precise measurement of the secondary mass.

The asymmetry in the masses of GW190814 means that the spin of the more massive object dominates contributions to $\chi_{\rm eff}$ and χ_p. As both $\chi_{\rm eff}$ and χ_p are tightly constrained, we are able to bound the primary spin of GW190814 to be $\chi_1 \leqslant 0.07$, as shown in Figure 6. This is the strongest constraint on the primary spin for any gravitational-wave event to date (Abbott et al. 2019a, 2020a, 2020d).

The joint posterior probability of the magnitude and orientation of χ_1 and χ_2 are shown in Figure 6. Deviations from uniform shading indicate a spin property measurement. The primary spin is tightly constrained to small magnitudes, but its orientation is indistinguishable from the prior distribution. The spin of the less massive object, χ_2, remains unconstrained; the posterior distribution is broadly consistent with the prior.

The final mass M_f and final dimensionless spin χ_f of the merger remnant are estimated under the assumption that the secondary is a BH. By averaging several fits calibrated to numerical relativity (Hofmann et al. 2016; Johnson-McDaniel et al. 2016; Healy & Lousto 2017; Jiménez-Forteza et al. 2017), we infer the final mass and spin of the remnant BH to be $25.6^{+1.1}_{-0.9}\,M_\odot$ and $0.28^{+0.02}_{-0.02}$, respectively. The final spin is lower than for previous mergers (Abbott et al. 2019a, 2020d), as expected from the low primary spin and smaller orbital contribution due to the asymmetric masses.

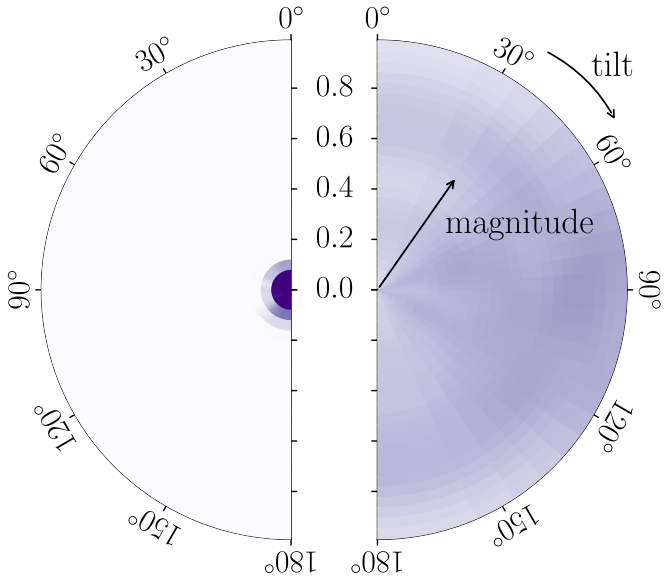

Figure 6. Two-dimensional posterior probability for the tilt-angle and spin-magnitude for the primary object (left) and secondary object (right) based on the combined samples. The tilt angles are 0° for spins aligned and 180° for spins antialigned with the orbital angular momentum. The tiles are constructed linearly in spin magnitude and the cosine of the tilt angles such that each tile contains identical prior probability. The color indicates the posterior probability per pixel. The probabilities are marginalized over the azimuthal angles.

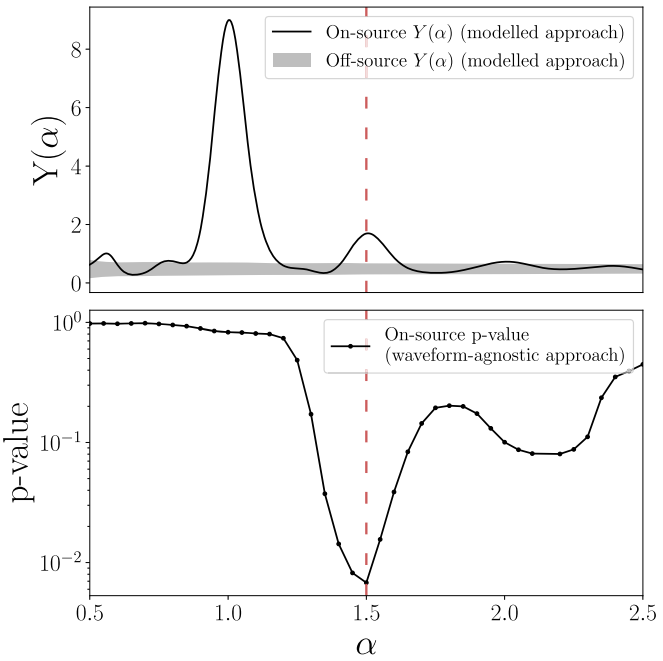

Figure 7. Top panel: variation of $Y(\alpha)$, i.e., the energy in the pixels along the α-th track defined by $f_\alpha(t) = \alpha f_{22}(t)$, using the modeled approach. The peaks at $\alpha = 1$ and 1.5 indicate the energies in the $m = 2$ and $m = 3$ multipoles, respectively. The gray band indicates the 68% confidence interval on the off-source measurements of $Y(\alpha)$. Bottom panel: the variation of p-value of the on-source results, as a function of α, using the waveform-agnostic approach. The dip at $\alpha = 1.5$ is strong evidence of the presence of the $m = 3$ mode in the underlying signal. The red dashed line in both panels corresponds to general relativity's prediction of $\alpha = 1.5$ for the $m = 3$ mode.

4.2. Evidence for Higher-order Multipoles

The relative importance of a subdominant multipole moment increases with mass ratio. Each subdominant multipole moment has a different angular dependence on the emission direction. With significant evidence for multipoles other than the dominant $(\ell, m) = (2, 2)$ quadrupole, we gain an independent measurement of the inclination of the source. This allows for the distance-inclination degeneracy to be broken (Cutler & Flanagan 1994; Abbott et al. 2016f; Kalaghatgi et al. 2020; Usman et al. 2019). Measuring higher-order multipoles therefore gives more precise measurements of source parameters (van den Broeck & Sengupta 2007a, 2007b; Kidder 2008; Blanchet et al. 2008; Mishra et al. 2016; Kumar et al. 2019).

GW190412 was the first event where there was significant evidence for higher-order multipoles (Kumar et al. 2019; Payne et al. 2019; Abbott et al. 2020d). GW190814 exhibits stronger evidence for higher-order multipoles, with $\log_{10}\mathcal{B} \simeq 9.6$ in favor of a higher-multipole versus a pure quadrupole model. The $(\ell, m) = (3, 3)$ is the strongest subdominant multipole, with $\log_{10}\mathcal{B} \simeq 9.1$ in favor of a signal model including both the $(\ell, m) = (2, 2)$ and $(3, 3)$ multipole moments. GW190814's stronger evidence for higher multipoles is expected given its more asymmetric masses and the larger network S/N.

The orthogonal optimal S/N of a subdominant multipole is calculated by decomposing each multipole into components parallel and perpendicular to the dominant harmonic (Abbott et al. 2020d; Mills & Fairhurst 2020). We infer that the orthogonal optimal S/N of the $(\ell, m) = (3, 3)$ multipole is $6.6^{+1.3}_{-1.4}$, as shown in Figure 5. This is the strongest evidence for measuring a subdominant multipole to date (Kumar et al. 2019; Payne et al. 2019; Abbott et al. 2020d).

Finally, we perform two complementary analyses involving time–frequency tracks in the data to provide further evidence for the presence of higher multipoles in the signal. In the first approach (also outlined in Abbott et al. 2020d, Section 4) we predict the time–frequency track of the dominant (2, 2) multipole in the LIGO Livingston detector (as seen in Figure 1, middle panel) from an EOBNR HM parameter estimation analysis. This analysis collects energies along a time–frequency track that is $\alpha \times f_{22}(t)$, the (2, 2) multipole's instantaneous frequency, where α is a dimensionless parameter (Roy et al. 2019b; Abbott et al. 2020d). We find prominent peaks in $Y(\alpha)$, the energy in the pixels along the α-th track defined in Abbott et al. (2020d), at $\alpha = 1$ and 1.5, as can be seen from the on-source curve in the top panel of Figure 7. These peaks correspond to the $m = 2$ and $m = 3$ multipole predictions in the data containing the signal (on-source data). We also compute a detection statistic β (Roy et al. 2019b) of 10.09 for the presence of the $m = 3$ multipole with a p-value of $<2.5 \times 10^{-4}$, compared to a background distribution estimated over 18 hr of data adjacent to the event (off-source data), where the largest background β is 7.59. The significant difference between on- and off-source values provides much stronger evidence for the presence of higher multipoles than what is reported for GW190412 (Abbott et al. 2020d).

The second analysis uses waveform-agnostic methods to reconstruct the signal. It then compares the observed coherent signal energy in the LIGO Hanford–LIGO Livingston–Virgo network of detectors, as identified by the cWB detection pipeline (Klimenko et al. 2016), with the predictions of a waveform model without higher multipoles (EOBNR; Prodi et al. 2020) to investigate if the description of the underlying signal is incomplete if we do not include contributions from the $m = 3$ multipole in our waveform model. We compute a test statistic, the squared sum of the coherent residuals estimated over

selected time–frequency tracks parameterized in terms of the same α parameter defined in the previous analysis (Roy et al. 2019b; Abbott et al. 2020d). Each time–frequency track centered on α includes frequencies within $[\alpha - 0.1,\ \alpha + 0.1] \times f_{22}(t)$, and times within $[t_{\rm merger} - 0.5$ s, $t_{\rm merger} - 0.03$ s], where $f_{22}(t)$ and $t_{\rm merger}$ correspond to the maximum likelihood template from the EOBNR parameter estimation analysis. We further compute a background distribution using simulated signals in off-source data (Prodi et al. 2020), and compute p-values for the on-source results as a function of α (Figure 7, bottom panel). We find a minimum p–value of 6.8×10^{-3} at $\alpha = 1.5$, providing strong evidence that the disagreement between the actual event and the EOBNR prediction is because of the absence of the $m = 3$ multipoles in the waveform model. The local minimum near $\alpha = 2$ is not an indication of the $m = 4$ multipoles, but rather a statistical fluctuation that is consistent with similar behavior seen for studies with simulated signals described in detail in Prodi et al. (2020).

Although the two time–frequency analyses are similar in motivation, the latter differs from the former in that it is not restricted to data from just one detector, but rather uses the coherent signal energy across the three-detector network. Both analyses point to strong evidence for the presence of higher multipoles in the signal.

5. Tests of General Relativity

GW190814 is the gravitational-wave event with the most unequal mass ratio to date, and can therefore be used to test general relativity (GR) in a region of parameter space previously unexplored with strong-field tests of GR (Abbott et al. 2016g, 2019e, 2019d). The asymmetric nature of a system excites the higher multipole moments of the gravitational signal, which allows us to test the multipolar structure of gravity (Kastha et al. 2018, 2019; Dhanpal et al. 2019; Islam et al. 2020). The addition of information from the higher harmonics of a signal also breaks certain degeneracies in the description of the source, and could potentially enable us to place stronger constraints on certain deviations from GR (van den Broeck & Sengupta 2007b, 2007a). We perform several null tests of GR using GW190814. These tests assume GW190814 is a (quasi-circular) BBH merger as described in GR, and look for inconsistencies between the observed signal and predictions of the theory. An inconsistency might arise from an incomplete understanding of the underlying signal (or noise), and could indicate a non-BBH nature of the signal or a potential departure from GR.

First, as a consistency test of the signal reconstruction, we subtract from the data the maximum likelihood compact binary coalescence waveforms, Phenom (Khan et al. 2016), Phenom HM (Kalaghatgi et al. 2020), Phenom PHM (Khan et al. 2020), and EOBNR PHM (Ossokine et al. 2020) and analyze 4 s of the resulting residual data centered around the time of merger with the morphology-independent transient analysis BAYESWAVE (Cornish & Littenberg 2015; Littenberg & Cornish 2015). We measure the 90% credible upper limit on the coherent S/N, ρ_{90}, and compare it to the S/N, ρ_{90}^N, recovered by analyzing 175 randomly selected data segments in surrounding time (off–source data) with the same configuration settings. If the residual data are consistent with the noise, we expect ρ_{90} to be consistent with ρ_{90}^N. We compute the p-value by comparing the distribution of ρ_{90}^N to ρ_{90} through $p = P(\rho_{90}^N < \rho_{90})$. We obtain p-values of 0.59, 0.82, 0.82, and 0.75 for Phenom, Phenom HM, Phenom PHM, and EOBNR PHM, respectively. Hence, we find no evidence for deviations in the behavior of the residual data stream.

We also look for deviations in the spin-induced quadrupole moments of the binary components. According to the no-hair conjecture (Carter 1971; Hansen 1974) the multipole moments of a Kerr BH are completely described by its mass and spin angular momentum. At leading order in spin, the spin-induced quadrupole moment scalar is (Hartle 1967; Pappas & Apostolatos 2012), $Q = -\kappa a^2 m^3$, where (m, a) are the mass and dimensionless spin of the compact object, and κ is a dimensionless deformation parameter characterizing deviations in the spin-induced quadrupole moment. Kerr BHs have $\kappa = 1$ (Thorne 1980), while $\kappa \sim 2$–14 for NSs (depending on the equation of state) and $\kappa \sim 10$–150 for spinning boson stars with large self-interaction (Ryan 1997). The deformation parameter can even be negative for (slowly rotating, thin-shelled) gravastars (Uchikata et al. 2016). Hence, an accurate measurement of κ sheds light onto the nature of the compact object. For compact binaries, the spin-induced quadrupole moment terms appear at second post-Newtonian order (Poisson 1998). For Kerr BHs in GR, $\kappa_1 = \kappa_2 = 1$, where κ_1, κ_2 are the individual deformation parameters of the primary and secondary compact objects in the binary. Since κ_1 and κ_2 are strongly degenerate in the gravitational waveform, we instead measure a linear symmetric combination of these quantities, $\kappa_{\rm s} = (\kappa_1 + \kappa_2)/2$, which is 1 for a BBH in GR. The posteriors on $\kappa_{\rm s}$ are relatively uninformative, and nearly span the prior range of [0, 500], with increased support at $\kappa_{\rm s} = 0$ relative to the prior. The upper bound of the prior was chosen to accommodate all the objects listed above. The result shows that GW190814 is consistent with having a BBH source described by GR. However, the broad posterior means that we cannot exclude the possibility that one or both components of the source is not a BH. We can attempt to understand this result in terms of the spin measurements for the binary. The measurements of $\kappa_{\rm s}$ and a nonzero $\chi_{\rm eff}$ are highly correlated (Krishnendu et al. 2019), and for a system with small $\chi_{\rm eff}$ the bounds on the measured value of $\kappa_{\rm s}$ are weak.

Finally, we investigate the source dynamics of the binary through a parameterized test of gravitational waveform generation, where we allow for the coefficients describing the post-Newtonian inspiral of a BBH coalescence to deviate away from their predictions in GR (Arun et al. 2006a, 2006b; Yunes & Pretorius 2009; Mishra et al. 2010; Cornish et al. 2011; Li et al. 2012; Meidam et al. 2018). We use an aligned-spin EOB waveform without higher modes (EOBNR), and find no deviations in the post-Newtonian coefficients from their nominal values in GR. In summary, none of our tests of GR indicate any departure from the predictions of the theory, and GW190814 is consistent with the description of a compact binary merger in GR.

6. Astrophysical Implications

The highly unequal mass ratio of $0.112^{+0.008}_{-0.009}$ and unusual secondary mass of $2.59^{+0.08}_{-0.09}\,M_\odot$ make the source of GW190814 unlike any other compact binary coalescence observed so far. The average mass ratio for BBH coalescences detected by the LVC during O1 and O2 is $\simeq$0.9 (Roulet & Zaldarriaga 2019), and an inference of the underlying population predicted that 99% of detectable BBHs have mass ratios $q \geqslant 0.5$ (Fishbach & Holz 2020). However, the paucity of events from O1 and O2 means that this picture is limited. Indeed, the discovery of GW190412 has already changed the picture substantially (Abbott et al. 2020d).

GW190814's secondary mass lies in the hypothesized lower mass gap of 2.5–5 $M_\odot$ (Bailyn et al. 1998; Özel et al. 2010; Farr et al. 2011; Özel et al. 2012) between known NSs and BHs. It is heavier than the most massive pulsar in the Galaxy (Cromartie et al. 2019), and almost certainly exceeds the mass of the 1.61–2.52 $M_\odot$ primary component of GW190425, which is itself an outlier relative to the Galactic population of BNSs (Abbott et al. 2020a). On the other hand, it is comparable in mass to two BH candidates: the $\simeq$2.7 $M_\odot$ merger remnant of GW170817 (Abbott et al. 2019b) and the 2.6–6.1 $M_\odot$ compact object (95% confidence interval) discovered by Thompson et al. (2019).[205] It is also comparable to the millisecond pulsar PSR J1748−2021B (Freire et al. 2008), whose mass is claimed as $2.74^{+0.21}_{-0.21}\,M_\odot$ at 68% confidence. However, this estimate, obtained via measurement of the periastron advance, could be inaccurate if the system inclination is low or the pulsar's companion is rapidly rotating (Freire et al. 2008). In sum, it is not clear if GW190814's secondary is a BH or an NS.

GW190814 poses a challenge for our understanding of the population of merging compact binaries. In what follows, we estimate the merger rate density of the compact binary subpopulation represented by this source, investigate the nature of its secondary component and possible implications for the NS equation of state, discuss how the system may have formed, and study its implications for cosmology.

6.1. Merger Rate Density

Given the unprecedented combination of component masses found in GW190814, we take the system to represent a new class of compact binary mergers, and use our analysis of its source properties to estimate a merger rate density for GW190814-like events. Following a method described in Kim et al. (2003), we calculate a simple, single-event rate density estimate $\mathcal{R}$ according to our sensitivity to a population of systems drawn from the parameter-estimation posteriors. As in Abbott et al. (2020a), we calculate our surveyed spacetime volume $\langle VT\rangle$ semianalytically, imposing single-detector and network S/N thresholds of 5 and 10, respectively (Tiwari 2018). The semianalytic $\langle VT\rangle$ for GW190814 is then multiplied by a calibration factor to match results from the search pipelines assuming a once-per-century FAR threshold. The sensitivity of a search pipeline is estimated using a set of simulated signals. For computational efficiency, this was done using preexisting search pipeline simulations and the mass properties were not highly optimized. However, given that we are estimating a rate based on a single source, the calibration errors are much smaller than the statistical errors associated with the estimate. The simulated sources were uniformly distributed in comoving volume, component masses, and component spins aligned with the orbital angular momentum. For O1 and O2, the simulated BH mass range was 5–100 $M_\odot$, but for the first part of O3 we are analyzing here, the injected range was 2.5–40 $M_\odot$ (following our updated knowledge of the BH mass distribution); the NS mass range was 1–3 $M_\odot$, and component spins are $<$0.95. As GW190814 occurred when LIGO Hanford was not in nominal observing mode, it is not included in the production PyCBC results, and we use GstLAL results to calculate the merger rate.

We assume a Poisson likelihood over the astrophysical rate with a single count and we apply a Jeffreys $\mathcal{R}^{-1/2}$ prior to obtain rate posteriors. The analysis was done using samples from the Phenom PHM posterior and separately from the EOBNR PHM posterior, producing the same result in both cases. We find the merger rate density of GW190814-like systems to be 7^{+16}_{-6} Gpc^{-3} yr^{-1}.

As a consistency check, we used the PyCBC search results to calculate an upper limit. Repeating the rate calculation with a PyCBC-based $\langle VT\rangle$ calibration and zero event count, we obtain an upper limit consistent (to within 10%) with the upper limit of the merger rate estimated using GstLAL search results. We conclude that the uncertainty in our estimate of the rate density for the class of mergers represented by GW190814 is primarily dominated by Poisson statistics.

6.2. Nature of the Secondary Component

The primary mass measurement of $23.2^{+1.1}_{-1.0}\,M_\odot$ securely identifies the heavier component of GW190814 as a BH, but the secondary mass of $2.59^{+0.08}_{-0.09}\,M_\odot$ may be compatible with either an NS or a BH depending on the maximum mass supported by the unknown NS equation of state (EOS). The source's asymmetric masses, the nondetection of an electromagnetic counterpart and the lack of a clear signature of tides or spin-induced quadrupole effects in the waveform do not allow us to distinguish between a BBH or an NSBH. Instead, we rely on comparisons between m_2 and different estimates of the maximum NS mass, $M_{\rm max}$, to indicate the source classification preferred by data: if $m_2 > M_{\rm max}$, then the NSBH scenario is untenable.

While some candidate EOSs from nuclear theory can support nonrotating NSs with masses of up to $\sim$3 $M_\odot$ (e.g., Müller & Serot 1996), such large values of $M_{\rm max}$ are disfavored by the relatively small tidal deformabilities measured in GW170817 (Abbott et al. 2017a, 2019b), which correlate with smaller internal pressure gradients as a function of density and hence a lower threshold for gravitational collapse. By adopting a phenomenological model for the EOS, conditioning it on GW170817, and extrapolating the constraints to the high densities relevant for the maximum mass, Lim & Holt (2019) and Essick et al. (2020) place $M_{\rm max} \lesssim 2.3\,M_\odot$. Similarly, the EOS inference reported in Abbott et al. (2018), based on an analysis of GW170817 with a spectral parameterization (Lindblom 2010; Lindblom & Indik 2012, 2014) for the EOS, implies a 90% credible upper bound of $M_{\rm max} \leqslant 2.43\,M_\odot$, with tenuous but nonzero posterior support beyond 2.6 $M_\odot$. We calculate the corresponding $M_{\rm max}$ posterior distribution, shown in the right panel of Figure 3, from the GW170817-informed spectral EOS samples used in Abbott et al. (2018) by reconstructing each EOS from its parameters and computing its maximum mass. Comparison with the m_2 posterior suggests that the secondary component of GW190814 is probably more massive than this prediction for $M_{\rm max}$: the posterior probability of $m_2 \leqslant M_{\rm max}$, marginalized over the uncertainty in m_2 and $M_{\rm max}$, is only 3%. Nevertheless, the maximum mass predictions from these kinds of EOS inferences come with important caveats: their extrapolations are sensitive to the phenomenological model assumed for the EOS; they use hard $M_{\rm max}$ thresholds on the EOS prior to account for the existence of the heaviest Galactic pulsars, which is known to bias the inferred maximum mass distribution toward the threshold (Miller et al. 2020); and they predate the NICER observatory's recent simultaneous mass and radius measurement for J0030+0451,

[205] See van den Heuvel & Tauris (2020) and Thompson et al. (2020b) for discussions about the interpretation of this observation.

which may increase the $M_{\rm max}$ estimates by a few percent (Landry et al. 2020) because it favors slightly stiffer EOSs than GW170817 (Miller et al. 2019; Raaijmakers et al. 2019; Riley et al. 2019; Jiang et al. 2020).

NS mass measurements also inform bounds on $M_{\rm max}$ independently of EOS assumptions. Fitting the known population of NSs in binaries to a double-Gaussian mass distribution with a high-mass cutoff, Alsing et al. (2018) obtained an empirical constraint of $M_{\rm max} \leqslant 2.6\,M_\odot$ (one-sided 90% confidence interval). Farr & Chatziioannou (2020) recently updated this analysis to include PSR J0740+6620 (Cromartie et al. 2019), which had not been discovered at the time of the original study. Based on samples from the Farr & Chatziioannou (2020) maximum-mass posterior distribution, which is plotted in the right panel of Figure 3, we find $M_{\rm max} = 2.25^{+0.81}_{-0.26}\,M_\odot$. In this case, the posterior probability of $m_2 \leqslant M_{\rm max}$ is 29%, again favoring the $m_2 > M_{\rm max}$ scenario, albeit less strongly because of the distribution's long tail up to $\sim 3\,M_\odot$. However, the empirical $M_{\rm max}$ prediction is sensitive to selection effects that could potentially bias it (Alsing et al. 2018). In particular, masses are only measurable for binary pulsars, and the mass distribution of isolated NSs could be different. Additionally, the discovery of GW190425 (Abbott et al. 2020a) should also be taken into account in the population when predicting $M_{\rm max}$.

Finally, the NS maximum mass is constrained by studies of the merger remnant of GW170817. Although no postmerger gravitational waves were observed (Abbott et al. 2017g, 2019f), modeling of the associated kilonova (Abbott et al. 2017b, 2017d; Cowperthwaite et al. 2017; Kasen et al. 2017; Villar et al. 2017) suggests that the merger remnant collapsed to a BH after a brief supramassive or hypermassive NS phase during which it was stabilized by uniform or differential rotation. Assuming this ultimate fate for the merger remnant immediately implies that no NS can be stable above $\sim 2.7\,M_\odot$, but it places a more stringent constraint on NSs that are not rotationally supported. The precise mapping from the collapse threshold mass of the remnant to $M_{\rm max}$ depends on the EOS, but by developing approximate prescriptions based on sequences of rapidly rotating stars for a range of candidate EOSs, $M_{\rm max}$ has been bounded below approximately 2.2–2.3 $M_\odot$ (Margalit & Metzger 2017; Rezzolla et al. 2018; Ruiz et al. 2018; Shibata et al. 2019; Abbott et al. 2020c). Although the degree of EOS uncertainty in these results is difficult to quantify precisely, if we take the more conservative $2.3\,M_\odot$ bound at face value, then m_2 is almost certainly not an NS: the m_2 posterior distribution has negligible support below $2.3\,M_\odot$.

Overall, these considerations suggest that GW190814 is probably not the product of an NSBH coalescence, despite its preliminary classification as such. Nonetheless, the possibility that the secondary component is an NS cannot be completely discounted due to the current uncertainty in $M_{\rm max}$.

There are two further caveats to this assessment. First, because the secondary's spin is unconstrained, it could conceivably be rotating rapidly enough for m_2 to exceed $M_{\rm max}$ without triggering gravitational collapse: rapid uniform rotation can stabilize a star up to ∼20% more massive than the nonrotating maximum mass (Cook et al. 1994), in which case only the absolute upper bound of $\sim 2.7\,M_\odot$ is relevant. However, it is very unlikely that an NSBH system could merge before dissipating such extreme natal NS spin angular momentum.

Second, our discussion has thus far neglected the possibility that the secondary component is an exotic compact object, such as a boson star (Kaup 1968) or a gravastar (Mazur & Mottola 2004), instead of an NS or a BH. Depending on the model, some exotic compact objects can potentially support masses up to and beyond $2.6\,M_\odot$ (Cardoso & Pani 2019). Our analysis does not exclude this hypothesis for the secondary.

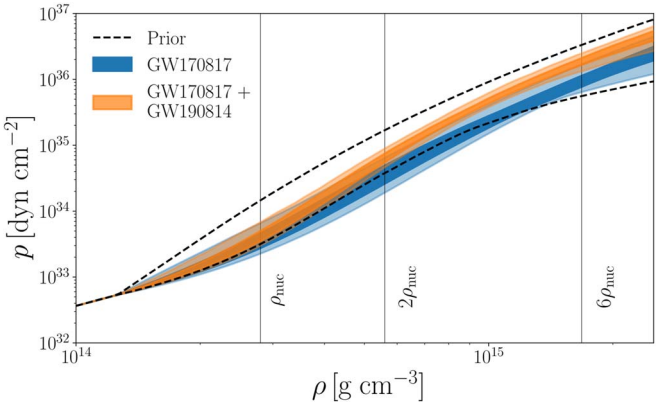

Figure 8. Constraints on the NS EOS assuming GW190814 was produced by a BBH (blue) or an NSBH (orange) coalescence. The 90% and 50% credible contours of the posterior in the pressure-density plane are shown. The constraints are calculated by assuming a spectral decomposition for the EOS, following Abbott et al. (2018). The BBH constraints are identical to those from the analysis of GW170817, while for the NSBH case the posterior is reweighted by the probability that each EOS's maximum mass is at least m_2. The dashed lines indicate the 90% credible region of the prior.

Since the NSBH scenario cannot be definitively ruled out, we examine GW190814's potential implications for the NS EOS, assuming that the secondary proves to be an NS. This would require $M_{\rm max}$ to be no less than m_2, a condition that severely constrains the distribution of EOSs compatible with existing astrophysical data. The combined constraints on the EOS from GW170817 and this hypothetical maximum mass information are shown in Figure 8. Specifically, we have taken the spectral EOS distribution conditioned on GW170817 from Abbott et al. (2018) and reweighted each EOS by the probability that its maximum mass is at least as large as m_2. The updated posterior favors stiffer EOSs, which translates to larger radii for NSs of a given mass. The corresponding constraints on the radius and tidal deformability of a canonical $1.4\,M_\odot$ NS are $R_{1.4} = 12.9^{+0.8}_{-0.7}$ km and $\Lambda_{1.4} = 616^{+273}_{-158}$.

6.3. Origins of GW190814-like Systems

The source of GW190814 represents a previously undetected class of coalescences that has the potential to shed light on the formation of merging compact-object binaries with highly asymmetric masses.

Electromagnetic observations of Galactic NSs and stellar-mass BHs suggest a dearth of compact objects in the $\sim 2.5\,M_\odot$ to $5\,M_\odot$ range (Bailyn et al. 1998; Özel et al. 2010; Farr et al. 2011; Özel et al. 2012). Observations of a few candidates with masses in this range seem to disfavor the existence of a gap (Freire et al. 2008; Neustroev et al. 2014; Giesers et al. 2018; Thompson et al. 2019; Wyrzykowski & Mandel 2020), but whether the mass gap is physical or caused by selection biases is still a matter of debate (e.g., Kreidberg et al. 2012).

From a theoretical point of view, accurately calculating the masses of compact remnants at formation is challenging, because it depends on the complex physics of the supernova

explosion and the details of stellar evolution, especially for the late evolutionary stages of massive stars (Janka 2012; Müller 2016; Burrows et al. 2018, 2019). Whether the models favor the presence of a gap or a smooth transition between NSs and BHs is still unclear, and in fact some models have been developed with the purpose of reproducing this lower mass gap (Ugliano et al. 2012; Fryer et al. 2012; Kochanek 2014; Sukhbold & Woosley 2014; Ertl et al. 2016). Therefore, our robust discovery of an object with a well-constrained mass in this regime may provide crucial constraints on compact-object formation models. In fact, GW190814 demonstrates the need to adjust remnant mass prescriptions previously designed to produce a perceived mass gap. The combination of mass ratio and component masses challenges most results obtained from population synthesis simulations for isolated binaries (Dominik et al. 2012, 2015; Marchant et al. 2017; Giacobbo & Mapelli 2018; Kruckow et al. 2018; Mapelli & Giacobbo 2018; Mapelli et al. 2019; Neijssel et al. 2019; Spera et al. 2019; Olejak et al. 2020).

Population synthesis models distinguish between NSs and BHs using only a mass threshold, which is generally in the range of 2–3 $M_\odot$. Thus, depending on the adopted threshold and on the adopted supernova explosion model, a GW190814-like event may be labeled as either an NSBH merger or a BBH merger. Most BBH mergers have $q > 0.5$, while the distributions of merging NSBH binaries suggest that systems with $q \lesssim 0.1$ may be up to $\sim 10^3$ times less common than more symmetric ones ($q > 0.1$) and that the mass-ratio distribution peaks at $q \approx 0.2$. Furthermore, models tend to favor mergers of massive ($\gtrsim 1.3\,M_\odot$) NSs with relatively small BHs ($\lesssim 15\,M_\odot$) in environments with subsolar metallicity ($Z \lesssim 0.5\,Z_\odot$). The tendency to disfavor mergers with highly asymmetric masses in isolated binaries may be the consequence of mass transfer (e.g., Postnov & Yungelson 2014) and common envelope episodes (e.g., Ivanova et al. 2013) that cause systems with initially asymmetric masses to evolve toward more symmetric configurations. Overall, producing mergers with such unequal masses, with a secondary in the perceived mass gap, and at the rate implied by this discovery is a challenge for current models.

Nevertheless, particular choices of poorly constrained assumptions within rapid population synthesis models may increase the number of mergers with $q \lesssim 0.1$ so that the latter may be only a few times less common than (or even comparable to) systems with $q \simeq 0.2$ (e.g., Eldridge & Stanway 2016; Eldridge et al. 2017; Giacobbo & Mapelli 2018).

Another possibility is that GW190814 is of dynamical origin. Dynamical exchanges in dense stellar environments tend to pair up massive compact objects with similar masses (e.g., Sigurdsson & Hernquist 1993). This process is effective for globular clusters, where compact-object binaries may undergo tens of exchanges before they get ejected from the cluster (Portegies Zwart & McMillan 2000; Rodriguez et al. 2016, 2019; Askar et al. 2017; Park et al. 2017). For such environments, models predict that most merging BBHs have $q \simeq 1$ (e.g., Rodriguez et al. 2016), and the formation of NSBH binaries is highly suppressed because BHs dynamically dominate the cores over the complete lifetime of the clusters, preventing the interactions between BHs and NSs, with the consequence that the merger rate of NSBH binaries in globular clusters in the local universe is $\sim 10^{-2}$–$10^{-1}\,\mathrm{Gpc^{-3}\,yr^{-1}}$ (Clausen et al. 2013; Arca Sedda 2020; Ye et al. 2020). The rate for GW190814-like events, with a secondary in the perceived mass gap, is likely even lower. In contrast, the NSBH merger rate may be significantly higher in young star clusters (e.g., Ziosi et al. 2014) and the latter can effectively increase the number of progenitors leading to merging compact-object binaries with $q \lesssim 0.15$ (di Carlo et al. 2019; Rastello et al. 2020). Thus, young star clusters may be promising hosts for GW190814-like events, but the parameter space relevant for GW190814 is mostly unexplored in the context of star clusters.

In dense stellar environments, GW190814-like systems may also form from a low-mass merger remnant that acquires a BH companion via dynamical interactions (Gupta et al. 2020). Gupta et al. (2020) predicts a population of second-generation BHs in the 2.2–3.8 $M_\odot$ range, with a peak in the distribution at 2.6 $M_\odot$, assuming a double-Gaussian mass distribution for the NSs. However, recent dynamical simulations of globular clusters (e.g., Ye et al. 2020) find the subsequent merger of such a second-generation BH with a larger stellar-mass BH to be exceedingly rare. A high component spin could be a distinguishing feature of a second-generation compact object, but the uninformative spin posterior for the lighter component of GW190814 provides no evidence for or against this hypothesis.

A GW190814-like merger may also have originated from a hierarchical triple in the field (e.g., Antonini et al. 2017; Silsbee & Tremaine 2017; Fragione & Loeb 2019), from a wide hierarchical quadruple system (Safarzadeh et al. 2020), or from hierarchical triples in galactic centers, where the tertiary body is a supermassive BH (Antonini & Perets 2012; Petrovich & Antonini 2017; Hoang et al. 2018; Fragione et al. 2019; Stephan et al. 2019). Specifically, Safarzadeh et al. (2020) explore the possibility that a second-generation remnant with mass 3 $M_\odot$ may merge with a 30 $M_\odot$ BH, catalyzed by a 50 $M_\odot$-BH perturber. The mass-ratio distributions of BBH and NSBH mergers from hierarchical systems are similar to those of field binaries and it is unclear whether hierarchies may enhance the formation of merging compact-object binaries with highly asymmetric masses (e.g., Silsbee & Tremaine 2017).

Disks of gas around supermassive BHs in active galactic nuclei may be promising environments for the formation of GW190814-like systems. For such environments, theoretical models show that merging compact-object binaries with asymmetric masses are likely, but cannot necessarily accommodate masses as low as the secondary mass of GW190814 (e.g., Yang et al. 2019). However, McKernan et al. (2020) show that the median mass ratio of NSBH mergers in active galactic nucleus disks may be as low as ~ 0.07.

We conclude that the combination of masses, mass ratio, and inferred rate of GW190814 is challenging to explain, but potentially consistent with multiple formation scenarios. However, it is not possible to assess the validity of models that produce the right properties but do not make quantitative predictions about formation rates, even at some order-of-magnitude level.

Young star clusters and active galactic nucleus disks seem to be more promising hosts for GW190814-like mergers, since both these environments may enhance the formation of either progenitors of or directly merging compact-object binaries with more asymmetric masses to relevant rates. In contrast, globular-cluster models provide more robust predictions, showing that GW190814-like mergers with such asymmetric masses are outliers in the population predictions, even though a revision of the remnant-mass prescription is still needed. Isolated binaries could prove possible progenitors provided similar revisions are

implemented. The importance of field multiples remains to be fully explored. Future gravitational-wave observations will provide further insights into the dominance of different channels.

6.4. Cosmological Implications

Luminosity distances inferred directly from observed gravitational-wave events can be used with measurements of source redshifts in the electromagnetic spectrum to constrain cosmological parameters (Schutz 1986). Redshifts can be either obtained directly from counterparts to the gravitational-wave source (Holz & Hughes 2005), as was the case for GW170817 (Abbott et al. 2017a, 2017b, 2017e), by cross-correlation of the gravitational-wave localization posterior with catalogs of galaxy redshifts (del Pozzo 2012; Chen et al. 2018; Nair et al. 2018; Abbott et al. 2019c; Gray et al. 2020; Fishbach et al. 2019; Soares-Santos et al. 2019), by exploiting information in the neutron star equation of state (Messenger & Read 2012), or by using the redshifted masses inferred from the gravitational wave observation and assumptions about the mass distribution of the sources (Chernoff & Finn 1993; Taylor et al. 2012; Taylor & Gair 2012; Farr et al. 2019). At current sensitivities, the cosmological parameter to which LIGO–Virgo observations are most sensitive is the Hubble constant, H_0. The gravitational-wave observation of GW170817 provided a posterior on H_0 with mode and 68.3% highest posterior density interval of $H_0 = 69^{+22}_{-8}$ km s^{-1} Mpc^{-1} (Abbott et al. 2017e, 2019b, 2019c), assuming a flat prior on H_0.

GW190814 is the best localized dark siren, i.e., gravitational-wave source without an electromagnetic counterpart, observed to date, and so it is a good candidate for the statistical cross-correlation method. For a fixed reference cosmology (Ade et al. 2016), the GLADE galaxy catalog (Dálya et al. 2018) is approximately 40% complete at the distance of GW190814 and contains 472 galaxies within the 90% posterior credible volume of GW190814. To obtain a constrain on H_0, we use the methodology described in Abbott et al. (2019c) and the GLADE catalog. We take a flat prior for $H_0 \in [20, 140]$ km s^{-1} Mpc^{-1} and assign a probability to each galaxy that it is the true host of the event that is proportional to its B-band luminosity. Using the posterior distribution on the distance obtained from the combined PHM samples, we obtain $H_0 = 75^{+59}_{-13}$ km s^{-1} Mpc^{-1} using GW190814 alone (mode and 68.3% highest posterior density interval; the median and 90% symmetric credible interval is $H_0 = 83^{+55}_{-53}$ km s^{-1} Mpc^{-1}), which can be compared to $H_0 = 75^{+40}_{-32}$ km s^{-1} Mpc^{-1} (Soares-Santos et al. 2019) obtained using the dark siren GW170814 alone. The GW190814 result is the most precise measurement from a single dark siren observation to date, albeit comparable to the GW170814 result, which is expected given GW190814's small localization volume ($\sim$39,000 Mpc^3). The result is not very constraining, with the 68.3% highest posterior density interval comprising 60% of the prior range. Combining the result for GW190814 with the result obtained from GW170817, we see an improvement over the GW170817-only result, to $H_0 = 70^{+17}_{-8}$ km s^{-1} Mpc^{-1} (the median and 90% symmetric credible interval is $H_0 = 77^{+33}_{-23}$ km s^{-1} Mpc^{-1}).This result is not yet sufficiently constraining to provide further insight into current tensions in low and high redshift measurements of the Hubble constant (Verde et al. 2019), but these constraints will continue to improve as further gravitational-wave observations are included (e.g., projections in Chen et al. 2018; Vitale & Chen 2018; Gray et al. 2020; Feeney et al. 2019).

7. Conclusions

During their third observing run, on 2019 August 14, 21:10:39 UTC, the LIGO and Virgo detectors observed GW190814, a novel source unlike any other known compact binary coalescence. Thanks in part to the observation of significant power in subdominant multipoles of the gravitational radiation, and the conclusive measurement of little to no spin precession, we obtain precise measurements of its physical source properties that clearly set it apart from other compact binaries.

In particular, (a) its mass ratio of $q = 0.112^{+0.008}_{-0.009}$ is the most unequal ever observed with gravitational waves, (b) the bound $\chi_1 \leqslant 0.07$ on the spin of the $23.2^{+1.1}_{-1.0}\,M_\odot$ BH is the strongest constraint on a primary spin for any gravitational-wave source to date, and (c) the secondary mass measurement of $2.59^{+0.08}_{-0.09}$ $M_\odot$ makes it the lightest BH or the heaviest NS discovered in a double compact-object system. We find no evidence of measurable tidal effects in the signal, and no electromagnetic counterpart to the gravitational waves has been identified.

Comparisons between the secondary mass and several current estimates of the maximum NS mass suggest that GW190814 is unlikely to originate in an NSBH coalescence. Nevertheless, the $M_{\rm max}$ estimates are uncertain enough that improved knowledge of the NS EOS or further observations of the astrophysical population of compact objects could alter this assessment. For this reason, we cannot firmly exclude the possibility that the secondary is an NS, nor can we be certain that it is a BH. Regardless, this event sheds new light on the compact-object mass distribution at the interface between known NSs and BHs.

The unique combination of masses and inferred merger rate for this event is difficult to produce in population synthesis models of multicomponent systems in galactic fields or dense stellar environments. The discovery of GW190814 may therefore reshape our understanding of the processes by which the lightest BHs or the most massive NSs form. Based on our rate density estimate, we may reasonably expect to detect more systems of this kind after a year at design sensitivity. This discovery may prove to be the first hint of a larger population that could change our perspective on the formation and mass spectrum of compact objects.

Segments of data containing the signal from all three interferometers, and samples from the posterior distributions for the source parameters, are available from the Gravitational Wave Open Science Center (https://doi.org/10.7935/zzw5-ak90). The software packages used in our analysis are open source.

The authors gratefully acknowledge the support of the United States National Science Foundation (NSF) for the construction and operation of the LIGO Laboratory and Advanced LIGO as well as the Science and Technology Facilities Council (STFC) of the United Kingdom, the Max-Planck-Society (MPS), and the State of Niedersachsen/Germany for support of the construction of Advanced LIGO and construction and operation of the GEO600 detector. Additional support for Advanced LIGO was provided by the Australian Research Council. The authors gratefully acknowledge the Italian Istituto Nazionale di Fisica Nucleare (INFN), the French Centre National de la Recherche Scientifique (CNRS) and the Netherlands Organization for Scientific Research, for the construction and operation of the Virgo detector and the creation and support of the EGO consortium.

The authors also gratefully acknowledge research support from these agencies as well as by the Council of Scientific and Industrial Research of India, the Department of Science and Technology, India, the Science & Engineering Research Board (SERB), India, the Ministry of Human Resource Development, India, the Spanish Agencia Estatal de Investigación, the Vicepresidència i Conselleria d'Innovació Recerca i Turisme and the Conselleria d'Educació i Universitat del Govern de les Illes Balears, the Conselleria d'Innovació Universitats, Ciència i Societat Digital de la Generalitat Valenciana and the CERCA Programme Generalitat de Catalunya, Spain, the National Science Centre of Poland, the Swiss National Science Foundation (SNSF), the Russian Foundation for Basic Research, the Russian Science Foundation, the European Commission, the European Regional Development Funds (ERDF), the Royal Society, the Scottish Funding Council, the Scottish Universities Physics Alliance, the Hungarian Scientific Research Fund (OTKA), the French Lyon Institute of Origins (LIO), the Belgian Fonds de la Recherche Scientifique (FRS-FNRS), Actions de Recherche Concertées (ARC) and Fonds Wetenschappelijk Onderzoek–Vlaanderen (FWO), Belgium, the Paris Île-de-France Region, the National Research, Development and Innovation Office Hungary (NKFIH), the National Research Foundation of Korea, Industry Canada and the Province of Ontario through the Ministry of Economic Development and Innovation, the Natural Science and Engineering Research Council Canada, the Canadian Institute for Advanced Research, the Brazilian Ministry of Science, Technology, Innovations, and Communications, the International Center for Theoretical Physics South American Institute for Fundamental Research (ICTP-SAIFR), the Research Grants Council of Hong Kong, the National Natural Science Foundation of China (NSFC), the Leverhulme Trust, the Research Corporation, the Ministry of Science and Technology (MOST), Taiwan and the Kavli Foundation. The authors gratefully acknowledge the support of the NSF, STFC, INFN and CNRS for provision of computational resources. Some of the parameter estimation analyses presented in this paper were performed using the supercomputer cluster at the Swinburne University of Technology (OzSTAR and SSTAR).

We would like to thank all of the essential workers who put their health at risk during the COVID-19 pandemic, without whom we would not have been able to complete this work.

Software: The detection of the signal and subsequent significance evaluation were performed with the GSTLAL-based inspiral software pipeline (Cannon et al. 2012; Privitera et al. 2014; Messick et al. 2017; Sachdev et al. 2019; Hanna et al. 2020), built on the LALSUITE software library (LIGO Scientific Collaboration 2018), and with the PYCBC (Nitz et al. 2018, 2019; Usman et al. 2016) and MBTAONLINE (Adams et al. 2016) packages. Parameter estimation was performed with the LALINFERENCE (Veitch et al. 2015) and LALSIMULATION libraries within LALSUITE (LIGO Scientific Collaboration 2018), as well as the BILBY and PBILBY Libraries (Ashton et al. 2019; Smith & Ashton 2019) and the DYNESTY nested sampling package (Speagle 2020). Interpretation and curation of the posterior samples was handled by the PESummary library (Hoy & Raymond 2020). Estimates of the noise spectra were obtained using BAYESWAVE (Cornish & Littenberg 2015; Littenberg & Cornish 2015). Plots were prepared with Matplotlib (Hunter 2007). The sky map plot also used Astropy (http://www.astropy.org) a community-developed core Python package for Astronomy (Astropy Collaboration et al. 2013; Price-Whelan et al. 2018) and `ligo.skymap` (https://lscsoft.docs.ligo.org/ligo.skymap).

ORCID iDs

S. Bernuzzi https://orcid.org/0000-0002-2334-0935
C. P. L. Berry https://orcid.org/0000-0003-3870-7215
M. Cabero https://orcid.org/0000-0003-4059-4512
N. Cornish https://orcid.org/0000-0002-7435-0869
D. E. Holz https://orcid.org/0000-0002-0175-5064
V. Kalogera https://orcid.org/0000-0001-9236-5469
J. S. Key https://orcid.org/0000-0003-0123-7600
K. Lee https://orcid.org/0000-0003-3175-1336
Shubhanshu Tiwari https://orcid.org/0000-0003-1611-6625
K. Ueno https://orcid.org/0000-0003-0424-3045
J. T. Whelan https://orcid.org/0000-0001-5710-6576
Hang Yu https://orcid.org/0000-0002-6011-6190
M. Zevin https://orcid.org/0000-0002-0147-0835

References

Aasi, J., Abbott, B. P., Abbott, R., et al. 2015, CQGra, 32, 074001
Abbott, B. P., Abbott, R., Abbott, T. D., et al. 2016a, PhRvL, 116, 061102
Abbott, B. P., Abbott, R., Abbott, T. D., et al. 2016b, PhRvX, 6, 041015
Abbott, B. P., Abbott, R., Abbott, T. D., et al. 2016c, CQGra, 33, 134001
Abbott, B. P., Abbott, R., Abbott, T. D., et al. 2016d, PhRvD, 93, 122003
Abbott, B. P., Abbott, R., Abbott, T. D., et al. 2016e, PhRvD, 93, 122004
Abbott, B. P., Abbott, R., Abbott, T. D., et al. 2016f, PhRvL, 116, 241102
Abbott, B. P., Abbott, R., Abbott, T. D., et al. 2016g, PhRvL, 116, 221101
Abbott, B. P., Abbott, R., Abbott, T. D., et al. 2017a, PhRvL, 119, 161101
Abbott, B. P., Abbott, R., Abbott, T. D., et al. 2017b, ApJL, 848, L12
Abbott, B. P., Abbott, R., Abbott, T. D., et al. 2017c, ApJL, 848, L13
Abbott, B. P., Abbott, R., Abbott, T. D., et al. 2017d, ApJL, 850, L39
Abbott, B. P., Abbott, R., Abbott, T. D., et al. 2017e, Nat, 551, 85
Abbott, B. P., Abbott, R., Abbott, T. D., et al. 2017f, ApJL, 851, L35
Abbott, B. P., Abbott, R., Abbott, T. D., et al. 2017g, ApJL, 851, L16
Abbott, B. P., Abbott, R., Abbott, T. D., et al. 2018, PhRvL, 121, 161101
Abbott, B. P., Abbott, R., Abbott, T. D., et al. 2019a, PhRvX, 9, 031040
Abbott, B. P., Abbott, R., Abbott, T. D., et al. 2019b, PhRvX, 9, 011001
Abbott, B. P., Abbott, R., Abbott, T. D., et al. 2019c, arXiv:1908.06060
Abbott, B. P., Abbott, R., Abbott, T. D., et al. 2019d, PhRvL, 123, 011102
Abbott, B. P., Abbott, R., Abbott, T. D., et al. 2019e, PhRvD, 100, 104036
Abbott, B. P., Abbott, R., Abbott, T. D., et al. 2019f, ApJ, 875, 160
Abbott, B. P., Abbott, R., Abbott, T. D., et al. 2020a, ApJL, 892, L3
Abbott, B. P., Abbott, R., Abbott, T. D., et al. 2020b, arXiv:1304.0670v10
Abbott, B. P., Abbott, R., Abbott, T. D., et al. 2020c, CQGra, 37, 045006
Abbott, R., Abbott, T. D., Abraham, S., et al. 2020d, arXiv:2004.08342
Accadia, T., Acernese, F., Antonucci, F., et al. 2010, CQGra, 27, 194011
Acernese, F., Adams, T., Agatsuma, K., et al. 2018, CQGra, 35, 205004
Acernese, F., Agathos, M., Agatsuma, K., et al. 2015, CQGra, 32, 024001
Ackley, K., Amati, L., Barbieri, C., et al. 2020, arXiv:2002.01950
Adams, T., Buskulic, D., Germain, V., et al. 2016, CQGra, 33, 175012
Ade, P. A. R., Aghanim, N., Arnaud, M., et al. 2016, A&A, 594, A13
Ageron, M., Baret, B., Coleiro, A., et al. 2019, GCN, 25330, 1
Ajith, P., Fotopoulos, N., Privitera, S., Neunzert, A., & Weinstein, A. J. 2014, PhRvD, 89, 084041
Ajith, P., Hannam, M., Husa, S., et al. 2011, PhRvL, 106, 241101
Alsing, J., Silva, H. O., & Berti, E. 2018, MNRAS, 478, 1377
Andreoni, I., Goldstein, D. A., Kasliwal, M. M., et al. 2020, ApJ, 890, 131
Antier, S., Agayeva, S., Aivazyan, V., et al. 2020, MNRAS, 492, 3904
Antonini, F., & Perets, H. B. 2012, ApJ, 757, 27
Antonini, F., Toonen, S., & Hamers, A. S. 2017, ApJ, 841, 77
Apostolatos, T. A., Cutler, C., Sussman, G. J., & Thorne, K. S. 1994, PhRvD, 49, 6274
Arca Sedda, M. 2020, CmPhy, 3, 43
Arun, K. G., Buonanno, A., Faye, G., & Ochsner, E. 2009, PhRvD, 79, 104023
Arun, K. G., Iyer, B. R., Qusailah, M. S. S., & Sathyaprakash, B. S. 2006a, PhRvD, 74, 024006
Arun, K. G., Iyer, B. R., Qusailah, M. S. S., & Sathyaprakash, B. S. 2006b, CQGra, 23, L37
Ashton, G., Hübner, M., Lasky, P. D., et al. 2019, ApJS, 241, 27
Askar, A., Szkudlarek, M., Gondek-Rosińska, D., Giersz, M., & Bulik, T. 2017, MNRAS, 464, L36

Astropy Collaboration, Robitaille, T. P., Tollerud, E. J., et al. 2013, A&A, 558, A33
Babak, S., Taracchini, A., & Buonanno, A. 2017, PhRvD, 95, 024010
Bailyn, C. D., Jain, R. K., Coppi, P., & Orosz, J. A. 1998, ApJ, 499, 367
Baird, E., Fairhurst, S., Hannam, M., & Murphy, P. 2013, PhRvD, 87, 024035
Blanchet, L. 2014, LRR, 17, 2
Blanchet, L., Damour, T., Esposito-Farèse, G., & Iyer, B. R. 2005, PhRvD, 71, 124004
Blanchet, L., Damour, T., Iyer, B. R., Will, C. M., & Wiseman, A. G. 1995, PhRvL, 74, 3515
Blanchet, L., Faye, G., Iyer, B. R., & Sinha, S. 2008, CQGra, 25, 165003
Bohé, A., Shao, L., Taracchini, A., et al. 2017, PhRvD, 95, 044028
Brown, D. A., Kumar, P., & Nitz, A. H. 2013, PhRvD, 87, 082004
Buonanno, A., & Damour, T. 1999, PhRvD, 59, 084006
Buonanno, A., Chen, Y., & Vallisneri, M. 2003, PhRvD, 67, 104025
Burrows, A., Radice, D., & Vartanyan, D. 2019, MNRAS, 485, 3153
Burrows, A., Vartanyan, D., Dolence, J. C., Skinner, M. A., & Radice, D. 2018, SSRv, 214, 33
Cannon, K., Cariou, R., Chapman, A., et al. 2012, ApJ, 748, 136
Capano, C., Dent, T., Hanna, C., et al. 2016a, PhRvD, 96, 082002
Capano, C., Harry, I., Privitera, S., & Buonanno, A. 2016b, PhRvD, 93, 124007
Cardoso, V., & Pani, P. 2019, LRR, 22, 4
Carter, B. 1971, PhRvL, 26, 331
Chatterji, S., Blackburn, L., Martin, G., & Katsavounidis, E. 2004, CQGra, 21, S1809
Chen, H.-Y., Fishbach, M., & Holz, D. E. 2018, Nat, 562, 545
Chernoff, D. F., & Finn, L. S. 1993, ApJL, 411, L5
Chornock, R., Berger, E., Kasen, D., et al. 2017, ApJL, 848, L19
Clausen, D., Sigurdsson, S., & Chernoff, D. F. 2013, MNRAS, 428, 3618
Cokelaer, T. 2007, PhRvD, 76, 102004
Cook, G. B., Shapiro, S. L., & Teukolsky, S. A. 1994, ApJ, 424, 823
Cornish, N., Sampson, L., Yunes, N., & Pretorius, F. 2011, PhRvD, 84, 062003
Cornish, N. J., & Littenberg, T. B. 2015, CQGra, 32, 135012
Cotesta, R., Buonanno, A., Bohé, A., et al. 2018, PhRvD, 98, 084028
Coughlin, M. W., Dietrich, T., Antier, S., et al. 2020, MNRAS, 492, 863
Cowperthwaite, P. S., Berger, E., Villar, V. A., et al. 2017, ApJL, 848, L17
Cromartie, H. T., Fonseca, E., Ransom, S. M., et al. 2019, NatAs, 4, 72
Cutler, C., & Flanagan, E. E. 1994, PhRvD, 49, 2658
Dálya, G., Galgóczi, G., Dobos, L., et al. 2018, MNRAS, 479, 2374
Damour, T. 2001, PhRvD, 64, 124013
Damour, T., Jaranowski, P., & Schäfer, G. 2001, PhLB, 513, 147
Davies, G. S., Dent, T., Tápai, M., et al. 2020, arXiv:2002.08291
del Pozzo, W. 2012, PhRvD, 86, 043011
Dhanpal, S., Ghosh, A., Mehta, A. K., Ajith, P., & Sathyaprakash, B. 2019, PhRvD, 99, 104056
di Carlo, U. N., Giacobbo, N., Mapelli, M., et al. 2019, MNRAS, 487, 2947
Dobie, D., Stewart, A., Murphy, T., et al. 2019, ApJL, 887, L13
Dominik, M., Belczynski, K., Fryer, C., et al. 2012, ApJ, 759, 52
Dominik, M., Berti, E., O'Shaughnessy, R., et al. 2015, ApJ, 806, 263
Effler, A., Schofield, R. M. S., Frolov, V. V., et al. 2015, CQGra, 32, 035017
Eldridge, J. J., & Stanway, E. R. 2016, MNRAS, 462, 3302
Eldridge, J. J., Stanway, E. R., Xiao, L., et al. 2017, PASA, 34, e058
Ertl, T., Janka, H. T., Woosley, S. E., Sukhbold, T., & Ugliano, M. 2016, ApJ, 818, 124
Essick, R., Landry, P., & Holz, D. E. 2020, PhRvD, 101, 063007
Fairhurst, S., Green, R., Hannam, M., et al. 2019a, arXiv:1908.00555
Fairhurst, S., Green, R., Hoy, C., et al. 2019b, arXiv:1908.05707
Farr, B., Berry, C. P. L., Farr, W. M., et al. 2016, ApJ, 825, 116
Farr, W. M., & Chatziioannou, K. 2020, RNAAS, 4, 65
Farr, W. M., Fishbach, M., Ye, J., & Holz, D. E. 2019, ApJL, 883, L42
Farr, W. M., Sravan, N., Cantrell, A., et al. 2011, ApJ, 741, 103
Feeney, S. M., Peiris, H. V., Williamson, A. R., et al. 2019, PhRvL, 122, 061105
Fernández, R., Foucart, F., & Lippuner, J. 2020, arXiv:2005.14208
Fishbach, M., Gray, R., Magaña Hernandez, I., Qi, H., & Sur, A. 2019, ApJL, 871, L13
Fishbach, M., & Holz, D. E. 2020, ApJL, 891, L27
Flanagan, E. E., & Hinderer, T. 2008, PhRvD, 77, 021502
Foucart, F., Buchman, L., Duez, M. D., et al. 2013, PhRvD, 88, 064017
Fragione, G., Grishin, E., Leigh, N. W. C., Perets, H. B., & Perna, R. 2019, MNRAS, 488, 47
Fragione, G., & Loeb, A. 2019, MNRAS, 486, 4443
Freire, P. C. C., Ransom, S. M., Bégin, S., et al. 2008, ApJ, 675, 670
Fryer, C. L., Belczynski, K., Wiktorowicz, G., et al. 2012, ApJ, 749, 91
Giacobbo, N., & Mapelli, M. 2018, MNRAS, 480, 2011
Giesers, B., Dreizler, S., Husser, T.-O., et al. 2018, MNRAS, 475, L15
Gomez, S., Hosseinzadeh, G., Cowperthwaite, P. S., et al. 2019, ApJL, 884, L55
Gray, R., Magaña Hernandez, I., Qi, H., et al. 2020, PhRvD, 101, 122001
Guo, X., Chu, Q., Chung, S. K., et al. 2018, CoPhC, 231, 62
Gupta, A., Gerosa, D., Arun, K. G., Berti, E., & Sathyaprakash, B. S. 2020, PhRvD, 101, 103036
Hanna, C., Caudill, S., Messick, C., et al. 2020, PhRvD, 101, 022003
Hansen, R. O. 1974, JMP, 15, 46
Harry, I. W., Allen, B., & Sathyaprakash, B. S. 2009, PhRvD, 80, 104014
Harry, I., Nitz, A. H., Brown, D. A., et al. 2014, PhRvD, 89, 024010
Hartle, J. B. 1967, ApJ, 150, 1005
Healy, J., & Lousto, C. O. 2017, PhRvD, 95, 024037
Hoang, B.-M., Naoz, S., Kocsis, B., Rasio, F. A., & Dosopoulou, F. 2018, ApJ, 856, 140
Hofmann, F., Barausse, E., & Rezzolla, L. 2016, ApJL, 825, L19
Holz, D. E., & Hughes, S. A. 2005, ApJ, 629, 15
Hooper, S., Chung, S. K., Luan, J., et al. 2012, PhRvD, 86, 024012
Hoy, C., & Raymond, V. 2020, arXiv:2006.06639
Huang, Y., Haster, C.-J., Vitale, S., et al. 2020, arXiv:2005.11850
Hunter, J. D. 2007, CSE, 9, 90
Husa, S., Khan, S., Hannam, M., et al. 2016, PhRvD, 93, 044006
Indik, N., Fehrmann, H., Harke, F., Krishnan, B., & Nielsen, A. B. 2018, PhRvD, 97, 124008
Islam, T., Mehta, A. K., Ghosh, A., et al. 2020, PhRvD, 101, 024032
Ivanova, N., Justham, S., Chen, X., et al. 2013, A&Ar, 21, 59
Janka, H.-T. 2012, ARNPS, 62, 407
Jiang, J.-L., Tang, S.-P., Wang, Y.-Z., Fan, Y.-Z., & Wei, D.-M. 2020, ApJ, 892, 55
Jiménez-Forteza, X., Keitel, D., Husa, S., et al. 2017, PhRvD, 95, 064024
Johnson-McDaniel, N. K., Gupta, A., Ajith, P., et al. 2016, Determining the final spin of a binary black hole system including in-plane spins: Method and checks of accuracy, Tech. Rep. LIGO-T1600168, https://dcc.ligo.org/T1600168/public
Kalaghatgi, C., Hannam, M., & Raymond, V. 2020, PhRvD, 10, 103004
Kapadia, S. J., Caudill, S., Creighton, J. D. E., et al. 2020, CQGra, 37, 045007
Karki, S., Tuyenbayev, D., Kandhasamy, S., et al. 2016, RScI, 87, 114503
Kasen, D., Metzger, B., Barnes, J., Quataert, E., & Ramirez-Ruiz, E. 2017, Nat, 551, 80
Kasliwal, M. M., Kasen, D., Lau, R. M., et al. 2019, MNRAS Letters, in press
Kasprzack, M., & Yu, H. 2017, Beam Position from Angle to Length Minimization, Tech. Rep. LIGO-T1600397, https://dcc.ligo.org/T1600397/public
Kastha, S., Gupta, A., Arun, K., Sathyaprakash, B., & van den Broeck, C. 2018, PhRvD, 98, 124033
Kastha, S., Gupta, A., Arun, K. G., Sathyaprakash, B. S., & van den Broeck, C. 2019, PhRvD, 100, 044007
Kaup, D. J. 1968, PhRv, 172, 1331
Kawaguchi, K., Shibata, M., & Tanaka, M. 2020, ApJ, 893, 153
Khan, S., Chatziioannou, K., Hannam, M., & Ohme, F. 2019, PhRvD, 100, 024059
Khan, S., Husa, S., Hannam, M., et al. 2016, PhRvD, 93, 044007
Khan, S., Ohme, F., Chatziioannou, K., & Hannam, M. 2020, PhRvD, 101, 024056
Kidder, L. E. 2008, PhRvD, 77, 044016
Kim, C., Kalogera, V., & Lorimer, D. R. 2003, ApJ, 584, 985
Klimenko, S., Yakushin, I., Mercer, A., et al. 2008, CQGra, 25, 114029
Klimenko, S., Vedovato, G., Drago, M., et al. 2016, PhRvD, 93, 042004
Kochanek, C. S. 2014, ApJ, 785, 28
Kreidberg, L., Bailyn, C. D., Farr, W. M., & Kalogera, V. 2012, ApJ, 757, 36
Krishnendu, N. V., Saleem, M., Samajdar, A., et al. 2019, PhRvD, 100, 104019
Kruckow, M. U., Tauris, T. M., Langer, N., Kramer, M., & Izzard, R. G. 2018, MNRAS, 481, 1908
Kumar, P., Blackman, J., Field, S. E., et al. 2019, PhRvD, 99, 124005
Kumar, P., Pürrer, M., & Pfeiffer, H. P. 2017, PhRvD, 95, 044039
Landry, P., Essick, R., & Chatziioannou, K. 2020, PhRvD, 101, 123007
Li, T. G. F., del Pozzo, W., Vitale, S., et al. 2012, PhRvD, 85, 082003
LIGO Scientific CollaborationVirgo Collaboration 2019a, GCN, https://gcn.gsfc.nasa.gov/notices_l/S190814bv.lvc
LIGO Scientific CollaborationVirgo Collaboration 2019b, Public Alerts User Guide, https://emfollow.docs.ligo.org/userguide/content.html
LIGO Scientific CollaborationVirgo Collaboration 2019c, GraceDB, S190814bv, https://gracedb.ligo.org/superevents/S190814bv/
LIGO Scientific CollaborationVirgo Collaboration 2019d, GCN, 25324, 1
LIGO Scientific CollaborationVirgo Collaboration 2019e, GCN, 25333, 1

LIGO Scientific Collaboration 2018, LIGO Algorithm Library, doi:10.7935/GT1W-FZ16
Lim, Y., & Holt, J. W. 2019, EPJA, 55, 209
Lindblom, L. 2010, PhRvD, 82, 103011
Lindblom, L., & Indik, N. M. 2012, PhRvD, 86, 084003
Lindblom, L., & Indik, N. M. 2014, PhRvD, 89, 064003
Lipunov, V., Gorbovskoy, E., Kornilov, V., et al. 2019, GCN, 25354, 1
Littenberg, T. B., & Cornish, N. J. 2015, PhRvD, 91, 084034
Liu, Y., Du, Z., Chung, S. K., et al. 2012, CQGra, 29, 235018
London, L., Khan, S., Fauchon-Jones, E., et al. 2018, PhRvL, 120, 161102
Mapelli, M., & Giacobbo, N. 2018, MNRAS, 479, 4391
Mapelli, M., Giacobbo, N., Santoliquido, F., & Artale, M. C. 2019, MNRAS, 487, 2
Marchant, P., Langer, N., Podsiadlowski, P., et al. 2017, A&A, 604, A55
Margalit, B., & Metzger, B. D. 2017, ApJL, 850, L19
Matas, A., Dietrich, T., Buonanno, A., et al. 2020, arXiv:2004.10001
Mazur, P. O., & Mottola, E. 2004, PNAS, 101, 9545
McKernan, B., Ford, K. E. S., & O'Shaughnessy, R. 2020, arXiv:2002.00046
Meidam, J., Tsang, K. W., Goldstein, J., et al. 2018, PhRvD, 97, 044033
Messenger, C., & Read, J. 2012, PhRvL, 108, 091101
Messick, C., Blackburn, K., Brady, P., et al. 2017, PhRvD, 95, 042001
Miller, M. C., Chirenti, C., & Lamb, F. K. 2020, ApJ, 888, 12
Miller, M. C., Lamb, F. K., Dittmann, A. J., et al. 2019, ApJL, 887, L24
Mills, J. C., & Fairhurst, S. 2020, Measuring gravitational-wave subdominant multipoles, Tech. Rep. LIGO-P2000136, https://dcc.ligo.org/P2000136/public
Mishra, C. K., Arun, K. G., Iyer, B. R., & Sathyaprakash, B. S. 2010, PhRvD, 82, 064010
Mishra, C. K., Kela, A., Arun, K. G., & Faye, G. 2016, PhRvD, 93, 084054
Morgan, R., Soares-Santos, M., Annis, J., et al. 2020, arXiv:2006.07385
Müller, B. 2016, PASA, 33, e048
Müller, H., & Serot, B. D. 1996, NuPhA, 606, 508
Nair, R., Bose, S., & Saini, T. D. 2018, PhRvD, 98, 023502
Neijssel, C. J., Vigna-Gómez, A., Stevenson, S., et al. 2019, MNRAS, 490, 3740
Neustroev, V. V., Veledina, A., Poutanen, J., et al. 2014, MNRAS, 445, 2424
Ng, K. K. Y., Vitale, S., Zimmerman, A., et al. 2018, PhRvD, 98, 083007
Nitz, A., Harry, I., Brown, D., et al. 2019, gwastro/pycbc: PyCBC Release v1.15.2, Zenodo, doi:10.5281/zenodo.3596447
Nitz, A. H., Dal Canton, T., Davis, D., & Reyes, S. 2018, PhRvD, 98, 024050
Nitz, A. H., Dent, T., Dal Canton, T., Fairhurst, S., & Brown, D. A. 2017, ApJ, 849, 118
Nitz, A. H., Dent, T., Davies, G. S., et al. 2020, ApJ, 891, 123
Nuttall, L. K. 2018, RSPTA, 376, 20170286
Olejak, A., Belczynski, K., Holz, D. E., et al. 2020, arXiv:2004.11866
Ossokine, S., Buonanno, A., Marsat, S., et al. 2020, arXiv:2004.09442
Owen, B. J. 1996, PhRvD, 53, 6749
Owen, B. J., & Sathyaprakash, B. S. 1999, PhRvD, 60, 022002
Özel, F., Psaltis, D., Narayan, R., & McClintock, J. E. 2010, ApJ, 725, 1918
Özel, F., Psaltis, D., Narayan, R., & Villarreal, A. S. 2012, ApJ, 757, 55
Pappas, G., & Apostolatos, T. A. 2012, PhRvL, 108, 231104
Park, D., Kim, C., Lee, H. M., Bae, Y.-B., & Belczynski, K. 2017, MNRAS, 469, 4665
Payne, E., Talbot, C., & Thrane, E. 2019, PhRvD, 100, 123017
Petrovich, C., & Antonini, F. 2017, ApJ, 846, 146
Poisson, E. 1998, PhRvD, 57, 5287
Poisson, E., & Will, C. M. 1995, PhRvD, 52, 848
Portegies Zwart, S. F., & McMillan, S. L. W. 2000, ApJL, 528, L17
Postnov, K. A., & Yungelson, L. R. 2014, LRR, 17, 3
Price-Whelan, A. M., Sipőcz, B. M., & Günther, H. M. 2018, AJ, 156, 123
Privitera, S., Mohapatra, S. R. P., Ajith, P., et al. 2014, PhRvD, 89, 024003
Prodi, G., Vedovato, G., Drago, M., et al. 2020, Technical note on the measurement of inspiral higher order modes by coherent WaveBurst in GW190814, Tech. Rep. LIGO-T2000124, https://dcc.ligo.org/T2000124/public
Pürrer, M. 2016, PhRvD, 93, 064041
Raaijmakers, G., Riley, T. E., Watts, A. L., et al. 2019, ApJL, 887, L22
Racine, E. 2008, PhRvD, 78, 044021
Rastello, S., Mapelli, M., di Carlo, U. N., et al. 2020, arXiv:2003.02277
Rezzolla, L., Most, E. R., & Weih, L. R. 2018, ApJL, 852, L25
Riley, T. E., Watts, A. L., Bogdanov, S., et al. 2019, ApJL, 887, L21
Rodriguez, C. L., Chatterjee, S., & Rasio, F. A. 2016, PhRvD, 93, 084029
Rodriguez, C. L., Zevin, M., Amaro-Seoane, P., et al. 2019, PhRvD, 100, 043027
Rosswog, S., Sollerman, J., Feindt, U., et al. 2018, A&A, 615, A132
Roulet, J., & Zaldarriaga, M. 2019, MNRAS, 484, 4216
Roy, S., Sengupta, A. S., & Ajith, P. 2019a, PhRvD, 99, 024048
Roy, S., Sengupta, A. S., & Arun, K. G. 2019b, arXiv:1910.04565
Roy, S., Sengupta, A. S., & Thakor, N. 2017, PhRvD, 95, 104045
Ruiz, M., Shapiro, S. L., & Tsokaros, A. 2018, PhRvD, 97, 021501
Ryan, F. D. 1997, PhRvD, 55, 6081
Sachdev, S., Caudill, S., Fong, H., et al. 2019, arXiv:1901.08580
Safarzadeh, M., Hamers, A. S., Loeb, A., & Berger, E. 2020, ApJL, 888, L3
Santamaría, L., Ohme, F., Ajith, P., et al. 2010, PhRvD, 82, 064016
Sathyaprakash, B., & Dhurandhar, S. 1991, PhRvD, 44, 3819
Schmidt, P., Ohme, F., & Hannam, M. 2015, PhRvD, 91, 024043
Schutz, B. F. 1986, Nat, 323, 310
Shibata, M., Zhou, E., Kiuchi, K., & Fujibayashi, S. 2019, PhRvD, 100, 023015
Sigurdsson, S., & Hernquist, L. 1993, Nat, 364, 423
Silsbee, K., & Tremaine, S. 2017, ApJ, 836, 39
Singer, L. P., & Price, L. 2016, PhRvD, 93, 024013
Smith, R., & Ashton, G. 2019, arXiv:1909.11873
Soares-Santos, M., Palmese, A., Hartley, W., et al. 2019, ApJL, 876, L7
Speagle, J. S. 2020, MNRAS, 493, 3132
Spera, M., Mapelli, M., Giacobbo, N., et al. 2019, MNRAS, 485, 889
Stephan, A. P., Naoz, S., Ghez, A. M., et al. 2019, ApJ, 878, 58
Sukhbold, T., & Woosley, S. E. 2014, ApJ, 783, 10
Tanvir, N. R., Levan, A. J., González-Fernández, C., et al. 2017, ApJL, 848, L27
Taylor, S. R., & Gair, J. R. 2012, PhRvD, 86, 023502
Taylor, S. R., Gair, J. R., & Mandel, I. 2012, PhRvD, 85, 023535
The IceCube Collaboration 2019, GCN, 25557, 1
Thompson, J. E., Fauchon-Jones, E., Khan, S., et al. 2020a, arXiv:2002.08383
Thompson, T. A., Kochanek, C. S., Stanek, K. Z., et al. 2019, Sci, 366, 637
Thompson, T. A., Kochanek, C. S., Stanek, K. Z., et al. 2020b, Sci, 368, eaba4356
Thorne, K. S. 1980, RvMP, 52, 299
Tiwari, V. 2018, CQGra, 35, 145009
Uchikata, N., Yoshida, S., & Pani, P. 2016, PhRvD, 94, 064015
Ugliano, M., Janka, H.-T., Marek, A., & Arcones, A. 2012, ApJ, 757, 69
Usman, S. A., Mills, J. C., & Fairhurst, S. 2019, ApJ, 877, 82
Usman, S. A., Nitz, A. H., Harry, I. W., et al. 2016, CQGra, 33, 215004
van den Broeck, C., & Sengupta, A. S. 2007a, CQGra, 24, 155
van den Broeck, C., & Sengupta, A. S. 2007b, CQGra, 24, 1089
van den Heuvel, E. P. J., & Tauris, T. M. 2020, Sci, 368, eaba3282
Veitch, J., Raymond, V., Farr, B., et al. 2015, PhRvD, 91, 042003
Venumadhav, T., Zackay, B., Roulet, J., Dai, L., & Zaldarriaga, M. 2020, PhRvD, 101, 083030
Verde, L., Treu, T., & Riess, A. G. 2019, NatAs, 3, 891
Vieira, N., Ruan, J. J., Haggard, D., et al. 2020, ApJ, 895, 96
Viets, A. D., Wade, M., Urban, A. L., et al. 2018, CQGra, 35, 095015
Villar, V. A., Guillochon, J., Berger, E., et al. 2017, ApJL, 851, L21
Vitale, S., & Chen, H.-Y. 2018, PhRvL, 121, 021303
Vitale, S., Lynch, R., Raymond, V., et al. 2017, PhRvD, 95, 064053
Vitale, S., Lynch, R., Veitch, J., Raymond, V., & Sturani, R. 2014, PhRvL, 112, 251101
Watson, A. M., Butler, N. R., Lee, W. H., et al. 2020, MNRAS, 492, 5916
Watson, D., Hansen, C. J., Selsing, J., et al. 2019, Nat, 574, 497
Wyrzykowski, Ł., & Mandel, I. 2020, A&A, 636, A20
Yang, Y., Bartos, I., Haiman, Z., et al. 2019, ApJ, 876, 122
Ye, C. S., Fong, W.-F., Kremer, K., et al. 2020, ApJL, 888, L10
Yunes, N., & Pretorius, F. 2009, PhRvD, 80, 122003
Zackay, B., Dai, L., Venumadhav, T., Roulet, J., & Zaldarriaga, M. 2019a, arXiv:1910.09528
Zackay, B., Venumadhav, T., Dai, L., Roulet, J., & Zaldarriaga, M. 2019b, PhRvD, 100, 023007
Ziosi, B. M., Mapelli, M., Branchesi, M., & Tormen, G. 2014, MNRAS, 441, 3703